High-accuracy calculation of parity nonconservation in cesium and implications for particle physics

S. A. Blundell*
University of California, Lawrence Livermore National Laboratory, P.O. Box 808, Livermore, California 94550

J. Sapirstein and W. R. Johnson
Department of Physics, University of Notre Dame, Notre Dame, Indiana 46556
(Received 28 October 1991)

High-precision measurements of atomic parity-nonconserving transitions in cesium when coupled with calculations of similar accuracy allow for a precise determination of Q_W, the weak nuclear charge. When expressed in terms of the Z mass, radiative corrections to Q_W are insensitive to the top-quark mass, so such a determination of Q_W allows a particularly sensitive probe of radiative corrections depending on new physics. While the wave function of cesium, the atom in which the most accurate measurements have been made, is extremely complex, atomic theory has advanced to a point where predictions accurate to 1% can be made. This paper describes such a calculation with particular emphasis on the question of the reliability of the atomic theory. Particle-physics implications following from the present state of theory and experiment are discussed, and prospects for more accurate work described.
PACS number(s): 31.10.+z, 12.15.Ji, 12.15.Mm, 35.10.Wb

I. INTRODUCTION

Modern field theory was brought into its present renormalizable form in the late 1940s largely through the stimulus provided by highly accurate atomic-physics measurements. Even before the direct measurement of the Lamb shift in hydrogen the effect had been seen in high-precision spectroscopy of the atom, and the existence of the electron's anomalous magnetic moment was first inferred from high-precision measurements of hyperfine splittings and g values in atoms. These and other radiative corrections have been measured with increasing accuracy over the years, and the very accurate agreement with theory found so far puts tight constraints on possible new physics at high energy scales, even though the energy scale of the atoms themselves is very small.

While QED has been tested to extremely high accuracy, with discrepancies between theory and experiment typically measured in parts per million (ppm), less accuracy has been achieved in the non-QED parts of the unified theories of weak and electromagnetic interactions. This is because, until recently, only one parameter governing the strength of weak interactions, G_F, was known with high accuracy (17 ppm). This situation has changed now that the mass of the Z has been measured [1] to the relatively high precision of 330 ppm. With the introduction of a third accurately known parameter of unified theories (the first being the fine-structure constant), it is now possible to make predictions of a large set of weak-interaction processes, assuming the validity of the standard model, that are sensitive to one-loop radiative corrections. In a certain sense, then, one is at the same stage of physics as described in the previous paragraph, where a theory successful at tree level can be tested with sufficient precision to require inclusion of radiative corrections.

There is an important difficulty in carrying out tests sensitive to radiative corrections in weak-interaction processes. That is the fact that the mass of the top quark, which is not at present directly known, enters significantly into these corrections. A similar, though less numerically important situation applies for the Higgs boson. As an example of this problem, if one wishes to use the Z mass measurement to determine the weak mixing angle in the modified minimal subtraction scheme [2], this value can vary by about 1.2% [3] as the top-quark mass is allowed to vary between 100 and 200 GeV:

$$\sin^2\hat{\theta}_W(m_W) = \begin{cases} 0.2328\,(5), & m_t = 100\ \text{GeV}, \\ 0.2301\,(4), & m_t = 200\ \text{GeV}. \end{cases} \quad (1)$$

While the top-quark mass can actually be constrained to a range around 140 GeV from consideration of other weak-interaction measurements, in particular the W-boson mass, it would clearly be desirable to find another weak-interaction process that is independent of this parameter. It happens that atomic parity nonconservation (PNC) in cesium, which was first discussed by Bouchiat and Bouchiat [4], is just such a process. This is because the quantity measured in atomic PNC experiments, the weak charge Q_W, when expressed as a function of the accurately known Z mass, has only a very weak dependence on the top-quark and Higgs-boson masses. For this reason, if an accurate measurement can be made, and if

*Present address: DRF/Service de Physique Atomique, CENG, 85X 38041 Grenoble Cedex, France.

the complex electronic structure of this atom can be convincingly calculated to the same accuracy, atomic physics could once again, as it did at the beginning of QED, play an important role in testing radiative corrections. The purpose of this paper is to discuss the possibility of this situation. Because an experiment accurate to 2% has been carried out by Wieman and collaborators [5], it is necessary to control the atomic structure calculation to under this level. We will present in this paper details of a calculation of PNC in cesium accurate to 1%. While work is in progress to reduce both the experimental and theoretical errors, we will see that already at the present level atomic physics is beginning to place constraints on technicolorlike theories [6, 7]. We note that PNC transitions have been measured in a number of other atoms [8], but we consider here only cesium as it is the simplest heavy atom to treat theoretically.

The plan of the paper is the following. We first in Sec. II give a brief overview of cesium PNC. Next, because the techniques of atomic many-body calculations may not be familiar to all readers interested in the particle-physics implications of atomic PNC, we introduce the basic methods of many-body perturbation theory (MBPT) in Sec. III, and apply it to the simplest many-electron atom, helium. This particularly simple atom can be studied with low orders of MBPT, but can also, with the introduction of what we call "all-order" methods, techniques that sum infinite classes of MBPT diagrams, be treated in an exact manner. One needs a method to carry out the infinite sums over states encountered in MBPT, and we use the simple helium example to illustrate the use of the relativistic finite basis set approach we have developed for both low orders of MBPT and the solution of all-order equations.

After this introduction to the techniques of relativistic MBPT, we turn to the calculation of energies and hyperfine constants in the far more complex atom we are interested in, cesium. We will show in Sec. III C that low orders of MBPT can achieve few percent accuracy, but that the more powerful all-order techniques are required to give agreement with experiment at better than the percent level.

After this general introduction we give the explicit details of two separate many-body calculations of PNC in Secs. IV and V. These two calculations, which form the central results of the paper, approach the calculation of PNC in very different ways. Therefore, in addition to performing tests to determine the likely level of error within each approach separately, we can also compare the results of the two calculations with each other. We find agreement within the one percent level that we quote as our overall theory error.

There are a number of smaller effects also entering at the one percent level that must be discussed before comparison with experiment can be made. We treat these effects in Sec. VI. In Sec. VII we compare with experiment, and we address the critical issue of the reliability of the atomic theory and prospects for improving it to the 0.1% level in Sec. VII A. We conclude in Sec. VIII with a discussion of the consequences of cesium PNC for particle physics.

II. OVERVIEW OF PNC IN CESIUM

The parity-nonconserving (PNC) electric-dipole amplitude has been measured for the $6S_{1/2} \rightarrow 7S_{1/2}$ transition in atomic cesium. Cesium is a 55 electron alkali-metal atom with one valence electron and a closed-shell xenon-like core. Because the core is relatively difficult to excite, this atom is one of the most tractable heavy atoms to treat theoretically. The experiment is sensitive only to the isotope ^{133}Cs, with $N = 78$ neutrons and $Z = 55$ protons. The nucleus has spin $I = 7/2$, which in the nuclear shell model arises from a single unpaired proton with Dirac angular quantum number $\kappa = 4$. The total angular momentum of the atomic S states is then either 3 or 4: the experiment measures both $6S(F = 3) \rightarrow 7S(F = 4)$ and $6S(F = 4) \rightarrow 7S(F = 3)$. These normally parity-forbidden transitions are allowed because of the exchange of a Z between the atomic electrons and the nucleus, and to a much smaller degree because of Z exchange between electrons. The dominant contribution comes from a vector coupling to the nucleus with an axial-vector coupling to the electrons (A_e, V_N), but smaller contributions arise from the reverse case (V_e, A_N). Because the nuclear vector current is conserved, the nucleus acts as a source of *weak charge*, denoted by Q_W. This weak charge is a combination of the vector coupling of the Z to up and down quarks, defined as

$$Q_W = 2Z(2C_{1u} + C_{1d}) + 2N(C_{1u} + 2C_{1d}), \tag{2}$$

where at tree level $C_{1u} = 1/2\,(1 - 8/3\sin^2\theta_W)$ and $C_{1d} = -1/2\,(1 - 4/3\sin^2\theta_W)$. The effect of the time-like component of the (A_e, V_N) part of Z exchange can then be described by the Hamiltonian

$$H_W = \frac{G_F}{\sqrt{8}} Q_W \rho_{\rm nuc}(\mathbf{r})\gamma_5 \tag{3}$$

with

$$Q_W = -N + Z(1 - 4\sin^2\theta_W). \tag{4}$$

The spacelike part is a small correction discussed in Sec. VI. Here $\rho_{\rm nuc}(\mathbf{r})$ is a weighted average of the proton and neutron distribution in the nucleus, and is discussed in Sec. VI B. This tree-level formula for Q_W is modified by radiative corrections, and an accurate determination of the weak charge can provide a test of these corrections. This Hamiltonian leads to a nonvanishing electric-dipole matrix element for the $6S_{1/2} \rightarrow 7S_{1/2}$ transition, the evaluation of which requires a large-scale atomic many-body calculation. We have carried out such a calculation (reported earlier in [9]) and determine the PNC dipole matrix element

$$E_{\rm PNC} = -0.905\,(9) \times 10^{-11}\, i|e|a_0(-Q_W/N)\,. \tag{5}$$

This equation is the central result of this paper. Note that allowed atomic dipole transitions are always proportional to $|e|a_0$: PNC transitions differ by being imaginary and greatly suppressed. Because Q_W is close to $-N$, it is conventional to express the result in terms of the ratio of the two numbers. The problem facing atomic theory

is the accurate prediction of the numerical coefficient in the above result.

Several experiments, all of which are consistent with one another, have measured PNC in cesium [5, 10–13]. The most accurate determination is [5]

$$E_{\rm PNC}/\beta = i\begin{cases} -1.513(50)\ {\rm mV/cm} & (F=3\rightarrow F'=4), \\ -1.639(48)\ {\rm mV/cm} & (F=4\rightarrow F'=3). \end{cases} \tag{6}$$

β is the vector transition polarizability for the $6S_{1/2}\rightarrow 7S_{1/2}$ transition, and is related to the electric dipole amplitude for the transition induced by an applied electric field [14]. It can be calculated in a manner similar to the calculation of $E_{\rm PNC}$, and the uncertainty in this quantity is part of the theoretical uncertainty in extracting Q_W. A difference between the two results given in Eq. (6) is expected because of nuclear spin-dependent effects, discussed in Sec. VI C. As discussed further in that section, a linear combination of the two measurements eliminates nuclear spin-dependent contributions, allowing a determination of the weak charge relatively free of nuclear physics uncertainties. The present result is $Q_W = -71.04\,(1.58)[0.88]$, where the first error is experimental and the second theoretical. This result is consistent with the theoretical prediction in the absence of new physics, $Q_W = -73.20(0.13)$. We discuss in Sec. VIII the implications of this situation for particle physics, the most important at present being the possibility of ruling out experimentally certain classes of technicolor theories of dynamical symmetry breaking [6, 7].

III. RELATIVISTIC MANY-BODY PERTURBATION THEORY

The ideal atomic system for the study of PNC would be hydrogen, because of its very well understood wave function. However, despite intense efforts, these experiments have not proved practical, so PNC must be studied in more complex atoms. Despite the fact that the underlying theory of atomic physics, QED, is well understood and successful for simple systems, the calculation of atomic properties in many-electron atoms is in no sense a straightforward or automatic task. This is because the many-body problem is extremely complex when a large number of particles are involved. This is most simply seen by imagining a table of an N-particle wave function with, say, an extremely coarse grid of 10 points per variable. After accounting for three free angular variables, 10^{3N-3} entries would be required, which clearly becomes unmanageable very rapidly.

Because there is no way the many-electron Dirac equation can be directly solved for cesium, some approximation scheme must be used to carry out calculations on this atom. Furthermore, because the PNC interaction takes place at small distances, being generated within the nuclear volume, this scheme should be relativistic. In addition, because we are interested in precision and reliable error estimates, a method that can be systematically improved is required. While there are a number of ways to address this problem, relativistic many-body perturbation theory has made the most progress so far, and will be discussed here exclusively. A given contribution of this perturbation theory can be represented by a time-ordered Feynman diagram, and will be referred to in the following as a diagram, short for Goldstone diagram. We will also discuss methods that sum infinite classes of diagrams, which we will refer to as "all-order" methods.

The basic problem we wish to solve is the many-electron Dirac equation with Hamiltonian $H \equiv H_C + H_{\rm Br}$, where

$$H_C \equiv \sum_{i=1}^{N}[\boldsymbol{\alpha}_i\cdot\mathbf{p}_i + \beta m + V_{\rm nuc}(r_i)] + \sum_{i<j}\frac{\alpha}{|\mathbf{r}_i-\mathbf{r}_j|} \tag{7}$$

and

$$H_{\rm Br} \equiv -\frac{\alpha}{2}\sum_{i<j}\frac{\boldsymbol{\alpha}_i\cdot\boldsymbol{\alpha}_j + \boldsymbol{\alpha}_i\cdot\hat{\mathbf{r}}_{ij}\,\boldsymbol{\alpha}_j\cdot\hat{\mathbf{r}}_{ij}}{|\mathbf{r}_i-\mathbf{r}_j|}. \tag{8}$$

Here $V_{\rm nuc}(r)$ represents the Coulomb potential of the nucleus. For helium we take this to be the potential of a point nucleus, but for cesium we account for the finite size of the nucleus using the Fermi distribution given in Eq. (70). The most important interaction in an atom is the Coulomb interaction, so H_C is treated as exactly as possible, and it usually suffices to treat magnetic interactions described by the Breit Hamiltonian $H_{\rm Br}$ as a perturbation. The many-electron Dirac equation actually has meaning only in the context of field theory, which provides a consistent set of rules for the treatment of retardation and negative-energy states. For the purposes of this paper, the simple rule of working with instantaneous interactions and leaving out negative-energy states in intermediate sums over states suffices. The latter rule prohibits unphysical transitions to the negative-energy sea that can occur when the many-electron Dirac equation is taken literally [15], and omits only small radiative corrections that can, if desired, be put back perturbatively. The Coulomb interaction is already instantaneous, and the neglect of retardation implicit in the use of Eq. (8) also corresponds to a small radiative correction.

Suppose one wanted to calculate the ground-state energy of the simplest many-electron atom, helium, starting from the Coulomb part of this Hamiltonian, with the condition that the method should be capable of extension to cesium. The procedure of MBPT is to first split H_C up into a lowest-order Hamiltonian in which each electron moves in some sort of averaged potential, and a perturbation that puts back in the complicated electron-electron interactions and also subtracts out the effect of the averaged potential. Specifically we write $H_C = H_0 + V_C$, where

$$H_0 \equiv \sum_{i=1}^{N}[\boldsymbol{\alpha}_i\cdot\mathbf{p}_i + \beta_i m + V_{\rm nuc}(r_i) + U(r_i)] \tag{9}$$

and

$$V_C \equiv \sum_{i<j}\frac{\alpha}{|\mathbf{r}_i-\mathbf{r}_j|} - \sum_{i=1}^{N}U(r_i). \tag{10}$$

For the purposes of illustrating the nature of MBPT calculations on two-electron atoms in this section we will make the simple choice $U(r) = 0$, which describes electrons moving in a Coulomb potential, with their mutual repulsion being treated as the perturbation. However, the averaged potential $U(r)$ is in principle completely arbitrary. It is of course desirable to choose a potential that gives a reasonable lowest-order description of the atom, and that also leads to a rapidly convergent perturbation expansion. It is possible to choose potentials with several adjustable parameters, generally referred to as model potentials. One approach to the many-body problem is to adjust these parameters so that some known properties of the atom, such as valence removal energies, are reproduced, and to then evaluate more complicated properties, such as PNC amplitudes, with the lowest-order wave functions obtained with these potentials. It is a remarkable fact that such an exercise can lead to predictions of radial matrix elements and hyperfine constants for cesium in agreement with experiment at the 10% level. However, it is essential to examine the behavior of the higher-order corrections to these potentials to gauge the accuracy of their predictions. We have done this for cesium, and found that model potentials that appear to reproduce energy levels at under the 1% level deteriorate significantly when studied in higher orders. On the other hand, the Hartree-Fock potential, while it reproduces energy levels relatively poorly in lowest order, typically being in error by 10% for valence removal energies, and between 20% and 50% for matrix elements, improves dramatically, to the few percent level for both energies and matrix elements, when two orders of MBPT are included. For this reason the calculations on cesium described below are carried out exclusively with the Hartree-Fock potential.

A. MBPT formulas

After choosing the potential $U(r)$, the solution of $H_0\psi_0 = E_0\psi_0$ is trivial, with the wave function being an antisymmetrized product of wave functions solved for in this potential, and the energy the sum of the respective eigenvalues. For a closed core system this wave function is represented as $|0_C>$, where, for example, ground state helium would be represented in terms of creation and annihilation operators as

$$|0_C> \equiv a^\dagger_{1s,m=1/2}a^\dagger_{1s,m=-1/2}|0>, \tag{11}$$

where $|0>$ is the vacuum, and because of the degeneracy of energy levels with different magnetic quantum numbers, $E_0 = 2\epsilon_{1s}$. When we later turn to cesium, the lowest-order wave function of a state with the valence electron in state v would be represented as

$$|v> = a^\dagger_v|0_C>, \tag{12}$$

where now $|0_C>$ refers to the configuration of xenon, and the lowest-order energy would be $E_0 = \epsilon_v + 2(\epsilon_{1s_{1/2}} + \epsilon_{2s_{1/2}} + \epsilon_{3s_{1/2}} + \epsilon_{4s_{1/2}} + \epsilon_{5s_{1/2}}) + 2(\epsilon_{2p_{1/2}} + \epsilon_{3p_{1/2}} + \epsilon_{4p_{1/2}} + \epsilon_{5p_{1/2}}) + 4(\epsilon_{2p_{3/2}} + \epsilon_{3p_{3/2}} + \epsilon_{4p_{3/2}} + \epsilon_{5p_{3/2}}) + 4(\epsilon_{3d_{3/2}} + \epsilon_{4d_{3/2}}) + 6(\epsilon_{3d_{5/2}} + \epsilon_{4d_{5/2}})$.

The lowest-order approximation for energies can be quite poor: for the example considered here, the ground-state energy of helium is $2\epsilon_{1s} = -4.000\,21$ a.u. [An atomic unit (a.u.) is two Rydbergs.] As the known value is $-2.903\,86$, it might be thought that perturbation theory would converge poorly. In fact, little is known about the convergence properties of MBPT from first principles. However, one can investigate this question empirically by carrying out calculations of low orders of MBPT. As will now be shown, practical experience shows that rather high accuracies can result starting from poor lowest-order results.

The formulas of MBPT can be derived in either a time-independent or time-dependent method. In the former one writes V_C in second quantized form as

$$V_C = \frac{1}{2}\sum_{ijkl} g_{ijkl}a^\dagger_i a^\dagger_j a_l a_k - \sum_{ij} U_{ij}a^\dagger_i a_j, \tag{13}$$

where g_{ijkl}, the Coulomb matrix element, is given by

$$g_{ijkl} = \alpha \int \frac{d^3r\, d^3r'}{|\mathbf{r}-\mathbf{r}'|}\bar{\psi}_i(\mathbf{r})\gamma_0\psi_k(\mathbf{r})\bar{\psi}_j(\mathbf{r}')\gamma_0\psi(\mathbf{r}'). \tag{14}$$

Sums over indices $i, j, k, \ldots$ are understood to range over all positive-energy states. It is also convenient in the following to adopt the convention that sums over $a, b, c, \ldots$ range over the occupied closed shells, and that sums over $m, n, r, \ldots$ refer to excited states, which include all states except the occupied closed shells. While nominally a six-dimensional integral, the angular integrals in Eq. (14) can be carried out analytically at the cost of introducing a partial-wave expansion, leaving a two-dimensional radial integral that is evaluated numerically. Because the partial-wave expansion converges rapidly, typically as $1/l^4$, inclusion of about seven partial waves along with an extrapolation to infinity allows for accurate evaluation of formulas involving Coulomb matrix elements. A frequently occurring combination of Coulomb matrix elements is

$$\tilde{g}_{ijkl} \equiv g_{ijkl} - g_{ijlk}, \tag{15}$$

where the first term is often referred to as the direct term, and the second the exchange term. An important use of this object is in the definition of the Hartree-Fock (HF) potential:

$$(V_{\rm HF})_{ij} \equiv \sum_a \tilde{g}_{iaja}. \tag{16}$$

At this point it is a straightforward exercise in Rayleigh-Schrödinger perturbation theory to derive formulas for corrections to the wave function, matrix elements, and energies [16]. For example, the first- and second-order energy corrections for a closed-shell system are

$$E^{(1)} = \sum_a (\tfrac{1}{2}V_{\rm HF} - U)_{aa} \tag{17}$$

and

$$E^{(2)} = \frac{1}{2}\sum_{abmn}\frac{g_{abmn}\tilde{g}_{mnab}}{\epsilon_{ab}-\epsilon_{mn}} + \sum_{am}\frac{(V_{\rm HF}-U)_{am}(V_{\rm HF}-U)_{ma}}{\epsilon_a-\epsilon_m}. \quad (18)$$

Here $\epsilon_{ij} \equiv \epsilon_i + \epsilon_j$, etc. For the case of helium, where for our potential $U = 0$, it is simple to evaluate

$$E^{(1)} = 1.250\,02, \quad (19)$$

which brings the MBPT result through first order to within 7% of the final answer. However, to achieve further precision $E^{(2)}$ must clearly be considered, which requires that a method to evaluate the summations in Eq. (18) be developed.

Before continuing with a discussion of how to evaluate these summations numerically, we discuss the time-dependent method of deriving MBPT formulas. This derivation involves the techniques of field theory, and while it reproduces the standard formulas of MBPT, it also allows a direct extension to a full QED implementation that allows the unambiguous identification of corrections to MBPT. The basic tool used in this approach is the Gell-Mann–Low formalism [17], in which V_C is turned off adiabatically at large positive and negative times via

$$V_C \to \lambda V_C e^{-\epsilon|t|}, \quad (20)$$

where λ is a quantity taken to unity at the end of any calculation. Contact with Feynman diagrams can be made by symmetrizing the original discussion of Ref. [17], which carried the wave function at large negative or positive time to time $t = 0$, to a form where the wave function is carried from large negative to large positive times [18]. This allows energy shifts to be expressed in terms of the S matrix via

$$\Delta E = \lim_{\epsilon\to 0}\frac{i\epsilon}{2}\frac{\partial}{\partial\lambda}\ln(< S_{\epsilon,\lambda} >_c)|_{\lambda=1}. \quad (21)$$

Use of this formalism with V_C upgraded to the full QED Hamiltonian then leads, when one considers graphs in which one photon is exchanged between electrons, to expressions like Eq. (17), but with retardation correctly built in, and when two photons are exchanged between electrons to expressions like Eq. (18). When the latter graphs are analyzed [19], after making a spectral decomposition of the two electron propagators, the contribution included in MBPT, with both intermediate summations of positive energy, is recovered. In addition negative-energy states can be seen to enter in a well defined way, that is, however, suppressed by a factor α^3. It is also possible to identify purely radiative corrections, such as the Lamb shift, which are also negligible for our purposes.

The sums over excited states can be efficiently carried out with the use of finite basis sets [20]. This technique, which is widely used in quantum chemistry, replaces the actual spectrum of the Dirac equation in a potential, which includes a continuum of negative-energy and positive-energy states along with an infinite number of bound states, with a pseudospectrum of typically around 100 states for each angular momentum state. The first step is to place the atom in a large cavity with MIT bag-model boundary conditions [21], which serves to discretize the continuum and limit the number of bound states. The Dirac action is then minimized with the restriction that each upper and lower component is expanded in terms of a finite number M of basis functions, which for this calculation were chosen to be B splines [22]. This minimization leads to an eigenvalue problem for the coefficients of the B splines and the associated energies, which leads to $2M$ eigenstates and energies, half of which approximate the negative-energy continuum and the remaining half the bound states and positive-energy continuum. The first few states in the positive-energy branch of the pseudospectrum accurately reproduce the lowest-lying bound-state energies and eigenvalues. We generally discard the negative-energy states in the calculations, though occasionally they need to be included.

With this basis set it is an easily automated task to evaluate Eq. (18). The result is

$$E^{(2)} = -0.157\,68, \quad (22)$$

which accounts for about 99.9% of the final answer. Higher orders of MBPT systematically give better and better agreement, as illustrated in Table I. Thus, in this particularly simple example, MBPT does indeed work. We will in Sec. III carry out low-order MBPT calculations for cesium, and will see a somewhat less pronounced pattern of convergence giving accuracies of a few percent.

B. All-order methods for helium

Suppose one wanted extremely high accuracy for the helium problem we have been discussing. While MBPT does converge systematically, even after going to fourth order one still is missing about 60 ppm of the complete result. Because of the rapid growth in the number of terms in the MBPT expansion, it is in general impractical to do a complete calculation past fourth order. However, there are a variety of methods that sum important classes of MBPT contributions to arbitrary order. We introduce them in the context of helium because for a two-electron system they are exact. The basic idea is to represent the exact helium ground state wave function as [23]

$$|\Psi>= N\left(1+\sum_{abij}{}'\rho_{ijab}a_i^\dagger a_j^\dagger a_a a_b\right)|0_C>, \quad (23)$$

TABLE I. Convergence of MBPT for ground-state helium. Units are a.u.

Order of MBPT	Energy	Cumulative Energy
$E^{(0)}$	−4.00021	−4.00021
$E^{(1)}$	1.25010	−2.75011
$E^{(2)}$	−0.15768	−2.90779
$E^{(3)}$	0.00434(NR) [a]	−2.90345
$E^{(4)}$	−0.00021(NR)	−2.90366
All orders		−2.90386(2)

[a]The nonrelativistic (NR) values are taken from J.J. Musher and J.M. Schulman, Phys. Rev. **173**, 93 (1968).

where the prime on the summation indicates that i and j cannot both be $1s$ states. Because no more than two core states can be destroyed for helium, this form encompasses all possible corrections to the wave function. By then operating on Eq. (23) with the Hamiltonian, and setting the result equal to $(E_0 + \Delta E)|\Psi>$, one obtains the equations

$$(\epsilon_{ij} - \epsilon_{ab} - \Delta E)\rho_{ijab} = \frac{1}{2} g_{ijab} - \sum_{kl}{}' g_{ijkl}\rho_{klab} \tag{24}$$

and

$$\Delta E = \frac{1}{2}\sum_{a}(V_{\rm HF})_{aa} - \sum_{abij}{}' \rho_{ijab}\tilde{g}_{abij} \, . \tag{25}$$

The first iterations of these equations reproduces the MBPT results of Eqs. (17) and (18), and higher iterations automatically reproduce the entire perturbation expansion. However, for a finite basis set the fundamental object ρ_{ijab} is simply a large matrix, and the above equations can be solved with standard iterative methods after angular reduction. It is relatively simple to get to the 1-ppm level with this method, and the result is shown in the last row of Table I. The numerical error quoted is dominated by uncertainties in the numerical extrapolation of the partial-wave summation to infinity, and can be reduced by including more partial waves.

C. Parity-conserving properties of cesium

We now turn to calculation of "ordinary," or parity-conserving properties of cesium using MBPT. A great deal is known about properties of this atom: a large number of energy levels have been measured with high precision, a fair number of hyperfine splittings have been measured, some with great accuracy (the ground-state hyperfine splitting serves as the standard of time), and oscillator strengths of a number of transitions are known with relatively poor accuracy. While not of interest for particle physics directly, these data are important because they allow us to test the behavior of MBPT. As will be discussed in more detail in Sec. VII A, the basic idea is that MBPT calculations of ordinary properties will agree with experiment only to a certain precision because of neglected terms. If all calculations of these properties in a given implementation of MBPT agree within, say, 1%, it is likely that, if the same implementation is extended to the PNC calculation, it will be accurate to about the same level. Hyperfine splitting is a particularly important property for this test, because, like PNC, it is generated at small distances. The actual error estimate for the PNC calculation involves in addition other tests, which are described further in Sec. IV B.

The first property we consider is the energy. Unlike the illustrative case of helium discussed above, we choose as our starting potential the frozen-core, or V^{N-1}, Hartree-Fock potential. The term frozen core refers to the fact that the Hartree-Fock equations are first solved for Cs^+, the $N-1$ electron system, which has the configuration of ground-state xenon. After these orbitals are determined they are held fixed, and the valence orbitals are then solved for in the HF potential given by Eq. (16). One advantage of this choice is that the different valence states we want to calculate are automatically orthogonal. In the V^N Hartree-Fock model, in which the valence electron contributes to the self-consistent potential, the core orbitals would be allowed to adjust to the valence electron, which would lead to a different set of core orbitals for each valence state, and different valence states would no longer be automatically orthogonal.

A particular simplification that results from this choice of the V^{N-1} Hartree-Fock potential is the vanishing of a large number of contributions involving $(V_{\rm HF} - U)_{ij}$. The first-order correction to the valence electron removal energy then vanishes, and the first correction to the energy is given by the formula

$$E^{(2)} = \sum_{mab}\frac{g_{mvba}\tilde{g}_{abmv}}{\epsilon_{ab} - \epsilon_{mv}} + \sum_{mna}\frac{g_{avmn}\tilde{g}_{mnav}}{\epsilon_{av} - \epsilon_{mn}} . \tag{26}$$

When evaluated with the same sort of methods described for helium, an improvement from the 10 to 1% level occurs, as can be seen from Table II. However, a qualitative difference between the helium and the cesium calculation is the fact that inclusion of the third order of MBPT actually leads to a deterioration rather than an improvement in the agreement with experiment. This can be traced to relatively large fourth-order diagrams that are in some sense iterations of the large second-order energy: when these are included agreement with experiment at the few tenths of a percent level is reached [24]. However, this is not a satisfactory situation, since other fourth-order

TABLE II. Convergence of MBPT for valence energies of cesium: units a.u.

Order of MBPT	$6s_{1/2}$	$6p_{1/2}$	$7s_{1/2}$
$E^{(0)}$	−0.12737	−0.08562	−0.05519
$E^{(2)}$	−0.01774	−0.00691	−0.00420
$E^{(3)}$	0.00563(17)	0.00163(10)	0.00139(4)
$E^{(4)}$ [b]	−0.00370(20)	−0.00148(8)	−0.00044(5)
$E_{\rm total}$	−0.14318(26)	−0.09238(13)	−0.05844(6)
$E_{\rm expt}$ [a]	−0.14310	−0.09217	−0.05865

[a] C.E. Moore, *Atomic Energy Levels*, Natl. Bur. Stand. Ref. Data Ser., Natl. Bur. Stand. (U.S.) Circ. No. 35 (U.S. GPO, Washington, D.C., 1971)

[b] Includes iterated Brueckner orbitals and fourth-order ladder graph as described in Ref. [24].

diagrams not included may also be large, and the agreement with experiment may be fortuitous. A complete catalog of all fourth-order diagrams would be of considerable value to explicitly find all large contributions, but this extremely large scale task (there are several hundred diagrams) has not been carried out. However, we will in the next section outline an all-order approach that can include all fourth-order diagrams, and a large set of fifth- and higher-order diagrams, that we believe will allow a very reliable calculation of all properties of cesium.

Before turning to these all-order methods, we discuss matrix elements. A general operator Z can be represented using second quantization as

$$Z = \sum_{ij} z_{ij} a_i^\dagger a_j . \tag{27}$$

If we denote the initial valence state as v and the final state as w, the matrix element of Z between these states has the MBPT expansion

$$< w|Z|v >= Z_{wv}^{(1)} + Z_{wv}^{(2)} + Z_{wv}^{(3)} + \cdots , \tag{28}$$

where $Z_{wv}^{(1)}$ and $Z_{wv}^{(2)}$ are given by

$$Z_{wv}^{(1)} = z_{wv} , \tag{29}$$

$$Z_{wv}^{(2)} = \sum_{i\neq v} \frac{z_{wi}(V_{\rm HF}-U)_{iv}}{\epsilon_v - \epsilon_i} + \sum_{i\neq w} \frac{z_{iv}(V_{\rm HF}-U)_{wi}}{\epsilon_w - \epsilon_i} + \sum_{am} \frac{z_{am}\tilde{g}_{wmva}}{\epsilon_{av} - \epsilon_{mw}} + \sum_{am} \frac{z_{ma}\tilde{g}_{wavm}}{\epsilon_{aw} - \epsilon_{mv}} . \tag{30}$$

The more complex formulas for $Z^{(3)}$ can be found in Ref. [16]: however, a particularly important set of terms are the *Brueckner orbital* (BO) corrections, given by

$$Z_{\rm BO}^{(3)} = \sum_{abmi} \left(\frac{g_{abmv} z_{wi} \tilde{g}_{imab}}{(\epsilon_i - \epsilon_v)(\epsilon_{mv} - \epsilon_{ab})} + \text{c.c.} \right) + \sum_{amni} \left(\frac{g_{aimn} z_{wi} \tilde{g}_{mnav}}{(\epsilon_i - \epsilon_v)(\epsilon_{mn} - \epsilon_{av})} + \text{c.c.} \right) , \tag{31}$$

where the notation c.c. means the complex conjugation of the previous expression combined with the interchange of v and w. These give particularly large corrections because the energy denominator $\epsilon_i - \epsilon_v$ can be relatively small, and when included with $Z^{(1)}$, $Z^{(2)}$, and higher-order random-phase-approximation (RPA) corrections, give results for ordinary matrix elements in agreement with experiment at the few percent level, as shown in Table III. At this point we can also illustrate one of the methods of carrying out a PNC calculation we have used. If the operator Z is chosen to be $D = |e|z$, we are dealing with the dipole operator that governs the strength of $E1$ transitions. If $v = 6S$ and $w = 7S$, parity-selection rules lead to a vanishing amplitude. However, when PNC interactions are introduced, the net effect is to give to each state a small opposite parity admixture:

$$|i>_\kappa \rightarrow |i>_\kappa + |i_{\rm PNC}>_{-\kappa} . \tag{32}$$

It is then a straightforward, though lengthy, procedure to make this substitution systematically for each state occurring in the MBPT formulas above, keeping only terms linear in $|i_{\rm PNC}>$, and to evaluate the resultant contribution to the PNC matrix element. This procedure was carried out in an earlier work [25], and the results are shown in Table III. It can be seen from that table that ordinary matrix elements are shifting by large amounts, but that after inclusion of second-order MBPT agreement with experiment at the 5% level is achieved. We will later see that the PNC number will shift by 4%, so the estimate of error given by monitoring ordinary matrix elements is in this case reliable. However, if information on radiative corrections is to be obtained, more accurate methods are clearly needed, and we now turn to the all-order methods used in this calculation.

D. All-order methods for cesium

We have shown in the simple case of helium an all-order method that allows an exact solution that encompasses all orders of MBPT. Unfortunately, this exactness relied on there being only two electrons in the atom. If one extends the method to even the simplest alkali-metal atom, lithium, Eq. (23) must be generalized to include a term involving three creation and three destruction operators, which we refer to as a *triples* term. For the large basis sets used in this work, storage of such a term is problematical. This method of expanding the wave function of an N electron system in terms of up to N destruction and N creation operators is equivalent to the *configuration interaction* method. The situation worsens with each additional electron, so that it is clearly impossible to generalize Eq. (23) to cesium. However, workers in quantum chemistry have found that terms with larger numbers of creation and annihilation operators are less and less numerically significant. In fact, rather accurate answers can usually be obtained by stopping at double excitations. Indeed, when the generalization of Eq. (23)

TABLE III. Convergence of MBPT for ordinary and PNC matrix elements of cesium. Units MHz for hyperfine, $|e|a_0$ for the allowed radial matrix element, and $i|e|a_0 10^{-11}(Q_W/-N)$ for the PNC matrix element.

Order of MBPT	$6s_{1/2}$ hyperfine	$7s_{1/2}$ hyperfine	$< 6p_{3/2}\|\|D\|\|6s_{1/2} >$	$< 7s_{1/2}\|\|D\|\|6s_{1/2} >$
$Z^{(1)}$	5740	1576	−7.426	−0.927
$Z_{\rm RPA}^{(2)}$	1156	320	0.413	0.037
$Z_{\rm BO}^{(3)}$	2568	392	0.842	−0.061
$Z_{\rm total}$	9464	2288	−6.171	−0.951
$Z_{\rm expt}$	9192	2184	−6.32(8)	

to alkali-metal atoms is made,

$$|\Psi>= N\Big(1+\sum_{am}\rho_{am}a_m^\dagger a_a+\sum_{abmn}\rho_{abmn}a_m^\dagger a_n^\dagger a_a a_b + \sum_m \rho_{vm}a_m^\dagger a_v + \sum_{avmn}\rho_{avmn}a_m^\dagger a_n^\dagger a_a a_v\Big)a_v^\dagger|0_C>, \quad (33)$$

extremely accurate predictions for lithium result [26], with energies accurate to 10 ppm and matrix elements to 0.1%. Unfortunately, when the same equation is applied to cesium, answers not much better than those obtained through second-order MBPT are found. We have traced this behavior to the fact that this method misses certain third-order MBPT diagrams that are negligible for lithium but relatively large for cesium. These diagrams are associated with the triples, and must either be put in perturbatively, or else the method generalized to include triples. We have partially carried out this latter step. This work, which is described in Ref. [27], is the basis of the present calculation of the PNC dipole amplitude. The basic idea is to add to the right-hand side of Eq. (33) the extra term

$$|\delta\Psi>= N\Big(\sum_{abcmnr}\rho_{abcmnr}a_m^\dagger a_n^\dagger a_r^\dagger a_a a_b a_c + \sum_{abmnr}\rho_{abmnr}a_m^\dagger a_n^\dagger a_r^\dagger a_a a_b a_v\Big)a_v^\dagger|0_C>. \quad (34)$$

When this is substituted into the many-electron Dirac equation the triple coefficients enter in two ways. First, there is a new equation for them that relates them to combinations of the single and double coefficients. Second, they alter the equations for those coefficients. We have at this point succeeded in accounting for the change in the singles equations caused by the introduction of the triples coefficient in an approximate way. The approximation has to do with the fact that we cannot store the triples coefficient. Instead we use the equation expressing it in terms of the singles and doubles to modify the right-hand side of the singles equation involving triples. Thus we are forced into the approximation of not iterating the triples coefficient. However, this method picks up all the missing third-order energy terms, and as discussed in connection with Table II, any method complete through third order that includes the important fourth-order energy contributions given in that table gives energies in agreement with experiment at the few tenths of a percent level. The present method, however, misses a large number of fourth-order diagrams, and it would be desirable to extend the method so that it is complete through this order. In order to do this, two steps are required. First, we must incorporate into Eq. (34) a special type of quadruple excitation, which can be factorized into a product of independent double excitations and modifies the doubles equation. The coupled-cluster method [28] provides an elegant way of handling these factorizable excitations. Second, the numerically very intensive problem of including the modification of the doubles equation due to triple excitations must be addressed. At this point the calculation will be complete through fourth order and will also include a large set of diagrams through infinite order. We expect our ability to calculate properties of cesium to improve to the 0.1% level once we have extended our method. However, for our present purposes of calculating cesium PNC to 1% our present method is already sufficient, and we now turn to a detailed description of two different methods of carrying out this calculation.

IV. SUM-OVER-STATES APPROACH

A. PNC dipole amplitude

Perhaps the most straightforward way to calculate the PNC electric dipole amplitude is to saturate the sum over N-body states X in the expression

$$E_{\rm PNC}=\sum_X\frac{<7S|D|X><X|H_{\rm PNC}|6S>}{E_{6S}-E_X}+\sum_X\frac{<7S|H_{\rm PNC}|X><X|D|6S>}{E_{7S}-E_X} \quad (35)$$

where $\mathbf{D}=\sum_{i=1}^N \mathbf{d}_i=\sum_{i=1}^N |e|\mathbf{r}_i$ is the dipole operator. This approach was used in some of the earliest calculations, and more recently in the semiempirical work of Bouchiat and Piketty [29]. Most of the sum—about 98%—comes from the four states $X=6P_{1/2}$, $7P_{1/2}$, $8P_{1/2}$, and $9P_{1/2}$, which in lowest order are described by a single valence $p_{1/2}$ electron outside the closed-shell core. In this first approach we use the accurate all-order procedure discussed above to calculate directly the matrix elements and energies of these four excited states. We refer to this contribution as the *main term* of the calculation. To complete the sum, we must also include the *tail* of the above sequence, $X=(10\text{–}\infty)P_{1/2}$, including the continuum, as well as autoionizing $P_{1/2}$ states, in which the core is excited. The tail contributes about 2% to the sum, the autoionizing states about -0.2%. Both of these smaller terms can be calculated to sufficient precision by simpler techniques than the all-order approach we use for the main term. Finally, we add the effect of the Breit interaction as one of the small corrections calculated in Sec. VI. We give a summary of the sum-over-states calculation in Table VII.

The explicit matrix elements and energies given by the all-order procedure [27] for $X=(6\text{–}9)P_{1/2}$ are summarized in Table IV. The sum can be seen to converge quite rapidly with respect to principal quantum n for $n\geq 8$, with only about 1.7% of the sum coming from the $9P_{1/2}$ state. We discuss how we estimate the theoretical uncertainty for these terms in the next section.

We now discuss in some detail the calculation of the tail, $X=(10\text{–}\infty)P_{1/2}$, which although contributing only about 2% turns out to be rather sensitive to many-body corrections and requires some care. Our method is a generalization of the lowest-order single-particle approximation to $E_{\rm PNC}$,

TABLE IV. Contributions to $E_{\rm PNC}$ from intermediate states $X = 6$–$9P_{1/2}$ in Eq. (35). Energies are experimental; matrix elements are taken from the all-order procedure with a fit to energies. Dipole matrix elements are of the form $< Xm = 1/2|D_z|Ym = 1/2 >$.

n	$\langle 7S\,\vert D\vert\, nP_{1/2}\rangle$ a.u.	$6S$ perturbed $\langle nP_{1/2}\,\vert H_{\rm PNC}\vert\, 6S\rangle$ $10^{-11}\, i(-Q_W/N)$ a.u.	$E_{6S} - E_{nP_{1/2}}$ a.u.	Contribution $10^{-11}\, i\vert e\vert a_0(-Q_W/N)$
6	1.7291	−0.0562	−0.05093	1.908
7	4.2003	0.0319	−0.09917	−1.352
8	0.3815	0.0215	−0.11714	−0.070
9	0.1532	0.0162	−0.12592	−0.020
n	$\langle 7S\,\vert H_{\rm PNC}\vert\, nP_{1/2}\rangle$	$7S$ perturbed $\langle nP_{1/2}\,\vert D\vert\, 6S\rangle$	$E_{7S} - E_{nP_{1/2}}$	Contribution
6	−1.8411	0.0272	0.03352	−1.493
7	0.1143	−0.0154	−0.01472	0.120
8	0.0319	−0.0104	−0.03269	0.010
9	0.0171	−0.0078	−0.04147	0.003
Total				−0.894

$$E_{\rm PNC}({\rm SP}) = \sum_{n=2}^{\infty} \frac{< 7s|d|np_{1/2} >< np_{1/2}|h_{\rm PNC}|6s >}{\epsilon_{6s} - \epsilon_{np_{1/2}}} + \left(\begin{matrix} d \leftrightarrow h_{\rm PNC} \\ \epsilon_{6s} \rightarrow \epsilon_{7s} \end{matrix}\right). \tag{36}$$

We adopt the convention that lower-case characters denote *single-particle* states. The sum here thus extends over all single-particle $p_{1/2}$ states and eigenvalues, and includes the occupied core $p_{1/2}$ states with $n = 2$–5. We evaluate this expression straightforwardly by summation over states of the finite basis set, identifying the lowest-order tail by restricting the summation to $n = 10$–∞. However, this lowest-order expression turns out to be quite inaccurate, because the continuum part of the sum is very sensitive to RPA corrections to the dipole operator. Once RPA terms have been included, however, the tail is quite insensitive to further many-body corrections. Including the RPA modifications Δd and $\Delta h_{\rm PNC}$ to the operators gives

$$E_{\rm PNC}({\rm tail}) = \sum_{n=10}^{\infty} \frac{< 7s|d + \Delta d|np_{1/2} >< np_{1/2}|h_{\rm PNC} + \Delta h_{\rm PNC}|6s >}{\epsilon_{6s} - \epsilon_{np_{1/2}}} + \left(\begin{matrix} d \leftrightarrow h_{\rm PNC} \\ \epsilon_{6s} \rightarrow \epsilon_{7s} \end{matrix}\right). \tag{37}$$

The RPA corresponds to an infinite sequence of screening or core polarization corrections to the operator, and may be calculated iteratively from the Dyson equation shown in Fig. 1. Explicitly, for an arbitrary one-body operator z,

$$z_{ij}^{\rm RPA}(\omega) \equiv z_{ij} + \Delta z_{ij}(\omega) = z_{ij} + \sum_{am} \left(\frac{\tilde{g}_{imja} z_{am}^{\rm RPA}(\omega)}{\epsilon_a - \omega - \epsilon_m} + \frac{\tilde{g}_{iajm} z_{ma}^{\rm RPA}(\omega)}{\epsilon_a + \omega - \epsilon_m} \right) \tag{38}$$

where a is an occupied core state, m is an excited state, and where ω is the energy difference of the two states involved in the matrix element. We have considered the approximation of fixing ω to a single value for the whole sum (37), for example, $\omega = E_{7S} - E_{6S}$ for dipole matrix elements and $\omega = 0$ for weak matrix elements. We find only a small error $\sim 0.1\%$ of $E_{\rm PNC}$ compared to the correct treatment in which ω varies according to the matrix element considered.

A subtlety arises in the evaluation of (37) connected with the size of the cavity used to discretize the continuum spectrum. One finds that the tail is quite sensitive to the cavity radius. For example, in lowest order the tail evaluates to $-0.0061 \times 10^{-11}\, i|e|a_0(-Q_W/N)$ for $r_{\rm cav} = 75$ a.u., which becomes $-0.0068 \times 10^{-11}\, i|e|a_0(-Q_W/N)$ as $r_{\rm cav} \rightarrow \infty$. On the other hand, the complete lowest-order sum for $n = 2$–∞, $E_{\rm PNC}({\rm SP}) = -0.740 \times 10^{-11}\, i|e|a_0(-Q_W/N)$, is essentially independent of the cavity radius for 70 a.u. $\leq r_{\rm cav} \leq$ 120 a.u.. Thus, while the total sum is very stable with respect to cavity size, the *distribution* of the sum between $n = 2$–9 and $n \geq 10$ varies quite markedly. Since we have used $r_{\rm cav} = 75$ a.u.

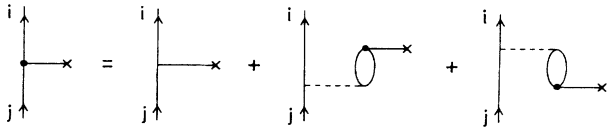

FIG. 1. Dyson equation for generating the RPA vertex for a one-body operator. The solid line terminated by a cross represents the operator, the dashed line represents the Coulomb interaction. Exchange terms (not shown) are also included.

for the main term, for consistency we also use $r_{cav} = 75$ a.u. in the tail calculation, even though this radius is not strictly physical.

We are now in a position to evaluate the RPA corrections to the tail by iterating the RPA equations and substituting into (37). We find that the lowest-order value of the tail, -0.0061, in the usual units of $10^{-11}\, i|e|a_0(-Q_W/N)$, changes by only a small amount, to -0.0078, upon inclusion of Δh_{PNC}, but by a large amount, to -0.019, upon inclusion of Δd. The tail contribution is thus seen to be very sensitive to RPA dipole terms, much more so in fractional terms than the total E_{PNC} (see Sec. V B).

While the RPA approximation includes the entire second-order contribution to a matrix element, it misses important terms in third order, whose effect on the tail we now estimate. One set of third-order terms are shown in Fig. 2, and discussed further in Sec. V D. Their inclusion in (37) modifies the tail to $-0.018 \times 10^{-11}\, i|e|a_0(-Q_W/N)$. A final important set of third-order terms is associated with the Brueckner orbital corrections (see Sec. V C) that were discussed in Sec. III C in connection with ordinary properties. We estimate the sensitivity of the tail to these terms by adding a semiempirical local potential $\delta V(r)$ to the HF potential with parameters adjusted to reproduce quite accurately the binding energies of the $6s$ and $7s$ states. The tail is modified by only about $0.002 \times 10^{-11}\, i|e|a_0(-Q_W/N)$. We take these third-order terms as an indication of the level of error in the tail, quoting $E_{PNC}(\text{tail}) = -0.018(4) \times 10^{-11}\, i|e|a_0(-Q_W/N)$. As the precision of the main terms improves, one may need a correspondingly more precise evaluation of the tail.

The contribution of autoionizing states may also be evaluated from the lowest-order expression (36) by restricting the sum to the occupied $p_{1/2}$ states. These core terms in the single-particle expression correspond to N-body states X in which a core $p_{1/2}$ state is excited to the $7s$ valence state. We find a contribution of order -0.2%, smaller than the present level of theory error. This result is fortunate because many-body corrections to these terms may be a substantial fraction of their lowest-order estimate, and are complicated to evaluate. We assign an error equal to the value of the term.

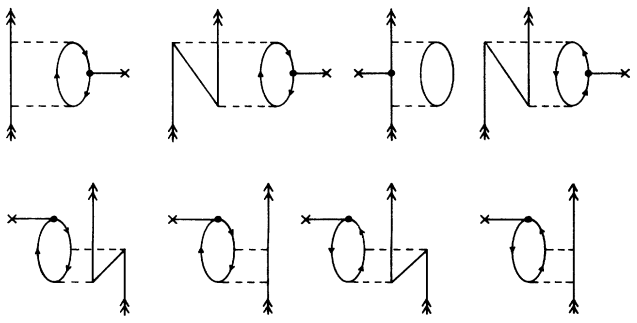

FIG. 2. Third-order "structural radiation" terms in the matrix element of a one-body operator. The solid line terminated by a cross represents the operator, the dashed line the Coulomb interaction.

B. Theoretical error in E_{PNC}

We have already discussed the level of error in the smaller terms in the calculation, the tail and autoionizing terms, but we now address the critical error estimation for the main term, which uses the all-order procedure. Because no rigorous error bounds are available for correlation calculations of this type, we estimate the error from the discrepancies with experiment found for the standard properties: energies, allowed dipole matrix elements and hyperfine constants. First, we note that since all standard properties relating directly to the PNC $6S$-$7S$ transition are predicted to better than 1% by our all-order procedure, it is likely that the PNC amplitude is also accurate to at least the 1% level. Our final conclusion is consistent with this statement. However, this simple argument may not be entirely reliable, because the quantity of interest, E_{PNC}, actually involves a rather complicated combination of matrix elements and energies. We have therefore performed a more detailed test of the likely theory error. Our procedure is to make plausible modifications to the all-order excitation coefficients (essentially to the wave function) to fit the experimentally determined standard properties, and then to evaluate E_{PNC} with the modified coefficients. These modifications essentially represent a semiempirical attempt to account for omitted correlation effects. By performing the various modifications listed below, we construct a set of different values for the main term, whose scatter we then take as the level of omitted correlation effects in the calculation. (See Table VI)

We consider five different types of modification to the all-order excitation coefficients, which we apply to the various quantities in Eq. (35) in the combinations summarized in Table VI. The five types of modifications are listed below as (i)–(v).

(i) *A fit to experimental ionization energies*, denoted by "e fit" in Table VI. An important class of omitted correlation effects in the matrix element calculation can be inferred from a comparison of ionization energies with experiment. As discussed above, the principal omissions in the all-order procedure are triple excitations and certain factorizable quadruple excitations. Now, the valence ionization energy is determined by the equation for valence single excitation coefficients ρ_{mv}, and these coefficients in turn largely control the Brueckner orbital (BO) correction M^{BO}, one of the biggest correlation effects in the matrix-element calculation. We find empirically a scaling relation, in which the valence correlation energy $\delta\epsilon_v$ and M^{BO} change in roughly the same fractions as different correlation terms are added to the all-order procedure. Thus we can estimate the sign and order of magnitude of omitted triple and quadruple excitations for M^{BO} by scaling the single excitation coefficients in the ratio $(\delta\epsilon_v)^{expt}/(\delta\epsilon_v)^{theory}$ and recalculating the matrix element.

(ii) *A fit to experimental hyperfine constants*, denoted by "hfs fit" in Table VI. Both the hyperfine interaction for $j = 1/2$ states and the weak electron-nucleus interaction act near the origin and are sensitive to the normalization of the wave function there. Normalization effects

TABLE V. Contributions to the scalar and vector $6S$–$7S$ transition polarizabilities α and β, and to the difference of Stark polarizabilities $\alpha_{7S} - \alpha_{6S}$, from intermediate states $(6\text{–}9)P_{1/2}$ and $(6\text{–}9)P_{3/2}$. Energies (not shown) are experimental; D denotes a reduced dipole matrix element calculated by the all-order procedure with a fit to ionization energies. Units are atomic units.

			$P_{1/2}$ channel		
n	$D(7S, nP_{1/2})$	$D(nP_{1/2}, 6S)$	α	β	α_{7S}-α_{6S}
6	4.236	-4.510	-32.46	-157.47	-311.5
7	10.289	0.280	-37.47	-27.79	2397.2
8	0.935	0.078	-0.48	-0.27	8.9
9	0.375	0.042	-0.08	-0.04	1.1
			$P_{3/2}$ channel		
n	$D(7S, nP_{3/2})$	$D(nP_{3/2}, 6S)$	α	β	α_{7S}-α_{6S}
6	-6.470	-6.347	-92.77	174.43	-701.4
7	14.293	-0.576	-102.09	37.31	4380.5
8	1.647	-0.214	-2.27	0.64	27.2
9	-0.725	0.132	-0.51	0.13	4.2
Total			-268.13	26.94	5806.2

are associated with the single-particle terms. Therefore we rescale M^{BO} to fit experimental hyperfine constants, and change the corresponding terms in the matrix element of h_{PNC} in the same ratio.

(iii) *A fit to experimental hyperfine constants* by scaling the *structural radiation* part M^{SR} of the matrix element, denoted by "sr fit" in Table VI. Here we consider the matrix element correction M^{SR}, which corresponds to the third-order terms in Fig. 2 evaluated with all-order coefficients rather than lowest-order Coulomb interactions [27]. Since some error in the matrix element calculation must be associated with double excitations, we somewhat arbitrarily rescale M^{SR} to fit experimental hyperfine constants, and rescale the corresponding terms for the weak matrix element in the same ratio.

(iv) *Direct use of experimental energies or dipole matrix elements in place of theoretical ones.* Generally, our theoretical dipole matrix elements appear to be at least as accurate as the measured values [27]. We therefore do not build the uncertainty in the measured dipole matrix elements into our theory error, but instead rely on the level of error indicated by the energy-fit analysis. One exception is the rather small but still quite important matrix elements of the type $< 7P|D|6S >$, for which correlation is quite large and where the measured value may be more reliable than our theoretical one. We indicate in a separate column in Table VI where experimental $< 7P|D|6S >$ values have been substituted.

(v) *Use of the dipole operator in velocity form rather than in length form.* When calculating dipole matrix elements, the velocity form of the dipole operator $\mathbf{d}_V = -ic|e|\boldsymbol{\alpha}/\omega_{fi}$, where ω_{fi} is the transition frequency, would be equivalent to the length form $\mathbf{d}_L = |e|\mathbf{r}$ if correlation were calculated exactly. We find quite close length-velocity agreement for dipole matrix elements using the all-order procedure [27]; as is shown in that reference, a significant improvement in length-velocity agreement results after a fit to ionization energies. Generally, the velocity form appears less suitable for correlation calculations because the corrections are larger and tend to cancel one another. We therefore do not place much weight on the values obtained by use of the velocity form, and have not included them in Table VI.

We should emphasize that here we consider calculating each dipole matrix element in (35) separately in velocity form, using the transition frequency ω_{fi} appropriate to that matrix element. An alternative implementation of length-velocity equivalence considers the $6S$–$7S$ transition directly, $< 7S + 7S_{\mathrm{PNC}}| \sum_{i=1}^{N} (d_i)_{\mathrm{L,V}} |6S + 6S_{\mathrm{PNC}} >$, with $\mathbf{d}_V = -ic|e|\boldsymbol{\alpha}/\omega_{7S,6S}$. In this approach, the dipole matrix elements in the sum over states are effectively multiplied by $\omega_{fi}/\omega_{7S,6S}$, and the corresponding main term lies well outside the range from tests (i)–(iv). The discrepancy is made up by positive- and negative-energy continuum states, whose contribution is enhanced by their large excitation energy.

The sum-over-states calculation is summarized in Table VII, and the scatter analysis in Table VI and Fig. 3. We combine the errors in the various terms in quadrature and find the final value

$$E_{\mathrm{PNC}}(\text{sum over states}) = -0.907(9) \times 10^{-11}\, i|e|a_0(-Q_W/N). \quad (39)$$

C. Vector transition polarizability β

An analogous sum-over-states approach can be applied to the other atomic quantity required to interpret the cesium experiment, the $6S$–$7S$ vector transition polarizability [14]:

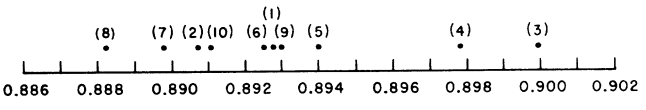

FIG. 3. Effect of modifying the calculation of the main term in various ways. The modifications are labeled according to the row in Table VI.

TABLE VI. Effect of modifying the calculation of the main term in various ways. D stands for dipole matrix elements, $h_{\rm PNC}$ for weak matrix elements, E for energies, and $D(7P,6S)$ for $7P$-$6S$ dipole matrix elements. The terms "e fit," "hfs fit," and "sr fit" are explained in the text; "raw" indicates the use of unmodified excitation coefficients or theoretical energies, "expt" denotes an experimental quantity. $E_{\rm PNC}$ is in units of $10^{-11}\,i|e|a_0(-Q_W/N)$; α, β, and $\alpha_{7S}-\alpha_{6S}$ are in atomic units. The values are plotted in Fig. 3.

	E	$h_{\rm PNC}$	D	$D(7P,6S)$	α	β	α_{7S}-α_{6S}	$E_{\rm PNC}$
1	Raw	Raw	Raw	Raw	-267.61	26.76	5918.7	-0.8928
2	Raw	Raw	Raw	Expt	-270.01	26.9	5918.6	-0.8908
3	Expt	Raw	Raw	Raw	-268.33	26.83	5864.8	-0.9000
4	Expt	Raw	Raw	Expt	-270.71	26.96	5864.7	-0.8979
5	Expt	e fit	e fit	e fit	-268.13	26.94	5806.2	-0.8943
6	Expt	e fit	e fit	Expt	-270.11	27.07	5806.1	-0.8926
7	Expt	hfs fit	e fit	e fit				-0.8898
8	Expt	hfs fit	e fit	Expt				-0.8882
9	Expt	sr fit	e fit	e fit				-0.8930
10	Expt	sr fit	e fit	Expt				-0.8910
Final					-268.0(3.0)	26.96(.20)	5830.(80.)	-0.893(7)

$$\beta = \frac{1}{6}\sum_{\gamma}\Bigg[< 7S||D||\gamma P_{1/2} >< \gamma P_{1/2}||D||6S > \left(\frac{1}{E_{7S}-E_{\gamma P_{1/2}}} - \frac{1}{E_{6S}-E_{\gamma P_{1/2}}}\right) + \frac{1}{2} < 7S||D||\gamma P_{3/2} >< \gamma P_{3/2}||D||6S > \left(\frac{1}{E_{7S}-E_{\gamma P_{3/2}}} - \frac{1}{E_{6S}-E_{\gamma P_{3/2}}}\right)\Bigg]. \tag{40}$$

We also calculate two quantities of similar structure to β for which experimental information is available to help gauge the accuracy of the procedure: the scalar transition polarizability [14]

$$\alpha = \frac{1}{6}\sum_{\gamma}\Bigg[< 7S||D||\gamma P_{1/2} >< \gamma P_{1/2}||D||6S > \left(\frac{1}{E_{7S}-E_{\gamma P_{1/2}}} + \frac{1}{E_{6S}-E_{\gamma P_{1/2}}}\right) - < 7S||D||\gamma P_{3/2} >< \gamma P_{3/2}||D||6S > \left(\frac{1}{E_{7S}-E_{\gamma P_{3/2}}} + \frac{1}{E_{6S}-E_{\gamma P_{3/2}}}\right)\Bigg]. \tag{41}$$

and the difference of the Stark polarizabilities of the $7S$ and $6S$ states,

$$\alpha_{7S}-\alpha_{6S} = -\frac{1}{3}\sum_{\gamma}\left(\frac{|< \gamma P_{1/2}||D||7S >|^2}{E_{7S}-E_{\gamma P_{1/2}}} + \frac{|< \gamma P_{3/2}||D||7S >|^2}{E_{7S}-E_{\gamma P_{3/2}}}\right) - (7S \to 6S). \tag{42}$$

A detailed breakdown for the main terms, with $(6\text{–}9)P$ intermediate states, is given in Table V. The convergence with respect to the principal quantum number is seen to be very fast, much faster than for $E_{\rm PNC}$. In Table VII we give the tail and autoionizing contributions, which we have calculated in a manner analogous to those for $E_{\rm PNC}$, although here they are negligible. We have also performed a scatter analysis to estimate the theoretical error of the main terms; the results are summarized in Table VI.

From Table VII, we find $(\alpha/\beta)^{\rm theory} = -9.93(14)$, in good agreement with the measurement [30] $(\alpha/\beta)^{\rm expt} =$

TABLE VII. Contributions to the scalar and vector transition polarizabilities α and β, the difference of Stark polarizabilities α_{7S}-α_{6S}, and the PNC dipole amplitude $E_{\rm PNC}$, in the sum-over-states approach. Polarizabilities are in atomic units, $E_{\rm PNC}$ is in units of $10^{-11}\,i|e|a_0(-Q_W/N)$.

	α	β	α_{7S}-α_{6S}	$E_{\rm PNC}$
(6-9P)	-268.0(3.0)	26.96(20)	5830.(80.)	-0.893(7)
(10–∞)P	-0.4(2)	0.04(2)	2	-0.018(5)
Autoionizing	0.4(4)	0.00	1.(1.)	0.002(2)
Breit	0.0	0.00	0	0.002
Total	-268.(3.)	27.00(.20)	5833.(80.)	-0.907(9)

$-9.9(1)$. For $\alpha_{7S}-\alpha_{6S}$, however, the agreement is not as satisfactory: our prediction $(\alpha_{7S}-\alpha_{6S})^{\text{theory}} = 5833(80)$ a.u. is to be compared with the measurement [31] $(\alpha_{7S}-\alpha_{6S})^{\text{theory}} = 5709(22)$. The quantity $\alpha_{7S}-\alpha_{6S}$ is controlled principally by dipole matrix elements of the form $< 7P|D|7S >$, which also play an important role in determining E_{PNC}. Dzuba, Flambaum, and Sushkov [32] have noted an analogous discrepancy between experiment and their theory for these dipole matrix elements. It is therefore of great interest to clarify the experimental situation, both as a guide to the accuracy of theoretical dipole matrix elements, and as a test of the reliability of the energy-fit procedure for estimating theoretical error.

Another quantity of experimental interest related to dipole matrix elements is the lifetime of the $7S$ state:

$$\frac{1}{\tau_{7S}} = \frac{2}{3}\frac{1}{c^3}\left(\omega^3_{7S,6P_{1/2}}|< 6P_{1/2}\|D\|7S >|^2 + \omega^3_{7S,6P_{3/2}}|< 6P_{3/2}\|D\|7S >|^2\right). \tag{43}$$

Using experimental frequencies and theoretical reduced dipole matrix elements from the all-order procedure [27], $< 6P_{1/2}\|D\|7S >= 4.228$ a.u. and $< 6P_{3/2}\|D\|7S >= 6.451$ a.u., we obtain $\tau_{7S}^{\text{theory}} = 48.8$ ns, in good agreement with the measurement by Bouchiat, Guena, and Pottier, [33] $\tau_{7S}^{\text{expt}} = 48.5(0.5)$ ns. This result is, however, in significant disagreement with an earlier measurement by Hoffnagle, Telegdi, and Weis [34], $\tau_{7S}^{\text{expt}} = 53.6(1.2)$ ns. The result of Ref. [33] is strongly favored theoretically: the use of HF level dipole matrix elements gives $\tau_{7S}^{\text{HF}} = 45.3$ ns, so that the result reported in Ref. [34] disagrees with theory by more than 100% of correlation.

We should also note that our value $\beta = 27.0(2)$ a.u. agrees with the semiempirical estimates $\beta = 27.2(4)$ a.u. by Bouchiat and Piketty [29], and $\beta = 27.3(4)$ a.u. by Gilbert and Wieman [13]. These authors first estimate α from (41) using experimental dipole matrix elements and energies, and a theoretical estimate for the tail for $n \geq 8$. They then infer β from a measurement of α/β. We also agree with the value of Bouchiat and Guena [35], $\beta = 27.17(35)$ a.u., obtained from a measurement of $M1^{\text{hfs}}/\beta$ and a semiempirical estimate of $M1^{\text{hfs}}$, the component of the $6S$–$7S$ magnetic dipole amplitude induced via the hyperfine interaction with the nucleus.

We find no significant correlation between the various modifications to β and E_{PNC}, so that the error in E_{PNC}/β is to be found by combining the separate errors.

V. PARITY-MIXED MANY-BODY APPROACH

A. Parity-mixed HF equations

As a check on the sum-over-states approach discussed above, we now calculate E_{PNC} in an entirely different way, using perturbed single-particle states [36]. This approach relies on the fact that the weak Hamiltonian h_{PNC} is of one-body form and can formally be included in the definition of the single-particle states, which become parity mixed. Since h_{PNC} is a pseudoscalar, the single-particle states remain eigenstates of angular momentum, however. Any conventional many-body method for calculating a dipole matrix element can then in principle be reformulated to use parity-mixed single-particle states in place of the usual parity-pure ones. It is usually convenient to linearize the resulting expressions in h_{PNC}. The method described below starts from a parity-mixed version of the HF equations, and then applies correlation corrections using a parity-mixed formulation of relativistic MBPT. The first complete calculation along the lines we describe was published by members of the Novosibirsk group [37, 32], although the general approach has a long history (recently reviewed by Blundell *et al.* [38]).

The parity-mixed HF equations are formed simply by adding h_{PNC} to the HF Hamiltonian:

$$\left(h_D + V_{\text{nuc}} + \tilde{V}_{\text{HF}} + h_{\text{PNC}}\right)\tilde{\psi} = \epsilon\tilde{\psi}. \tag{44}$$

The state $\tilde{\psi} = \psi + \psi_{\text{PNC}}$ here is a parity-mixed core or excited single-particle state, with ψ_{PNC} being the small opposite-parity admixture induced by h_{PNC}. The parity-mixed HF potential $\tilde{V}_{\text{HF}}$ is defined similarly to the usual HF potential, but involves parity-mixed core orbitals $|\tilde{c}\rangle$,

$$< i|\tilde{V}_{\text{HF}}|j >= \sum_{\tilde{c}}\left(< i\tilde{c}|r_{12}^{-1}|j\tilde{c} > - < i\tilde{c}|r_{12}^{-1}|\tilde{c}j >\right). \tag{45}$$

We must then solve (44) self-consistently, which we do by linearizing in h_{PNC} to give a pair of equations, the first of which is the usual HF equation

$$(h_D + V_{\text{nuc}} + V_{\text{HF}})\,\psi = \epsilon\psi, \tag{46}$$

$$(\epsilon - h_D - V_{\text{nuc}} - V_{\text{HF}})\,\psi_{\text{PNC}} = (h_{\text{PNC}} + V_{\text{PNC-HF}})\,\psi. \tag{47}$$

The PNC-HF potential $V_{\text{PNC-HF}}$ on the right-hand side (RHS) of (47) is the part of $\tilde{V}_{\text{HF}}$ linear in h_{PNC}. The energy eigenvalue ϵ is unaffected by h_{PNC} to first order since $< \psi|h_{\text{PNC}}|\psi >= 0$. At this level of approximation E_{PNC} is given by

$$E_{\text{PNC}}(\text{PNC-HF}) =< 7s|d|6s_{\text{PNC}} > + < 7s_{\text{PNC}}|d|6s > . \tag{48}$$

We solve (46) and (47) by conventional point-by-point integration techniques and obtain $E_{\text{PNC}}(\text{PNC-HF}) = -0.927\times 10^{-11}\, i|e|a_0(-Q_W/N)$. This result is now well-established (see Table VIII).

Because the result at PNC-HF level is only about 3% different from the final result (39), correlation corrections are small and the parity-mixed MBPT approach appears attractive. The parity-mixed HF method in fact already builds in the most important class of many-body effects beyond the lowest-order single-particle approximation (36). The latter approximation is equivalent to solving (47) with $V_{\text{PNC-HF}} = 0$, and gives $E_{\text{PNC}}(\text{SP}) = -0.740\times 10^{-11}\, i|e|a_0(-Q_W/N)$, 20% different from the PNC-HF result. The extra self-consistent term $V_{\text{PNC-HF}}$ in the PNC-HF approach has the effect of summing the

TABLE VIII. Contributions to $E_{\rm PNC}$ from parity-mixed MBPT. $E_{\rm PNC}$ is in units of $10^{-11}\, i|e|a_0(-Q_W/N)$.

Term	Present	Novosibirsk [a]	Gothenburg [b]
PNC-HF	−0.927		−0.927
RPA (external)	0.035		0.035
RPA (internal)	0.002	−0.886[c]	0.002
BO	−0.015(9)	−0.022	
BO-3 (internal)	−0.003	−0.003	
SR	−0.004(1)	−0.003	
Normalization	0.008	0.006	
Breit	0.002(2)		
Total	−0.902(9)	−0.908(10)	

[a] Reference [32].
[b] Reference [45]. These authors have also calculated the cross term between the RPA and the linearized BO correction to the valence states.
[c] This value represents the sum of PNC-HF, RPA (external), and RPA (internal).

important RPA corrections to $h_{\rm PNC}$, since one may show that $V_{\text{PNC-HF}} = \Delta h_{\rm PNC}(0)$, where $\Delta h_{\rm PNC}(\omega)$ is defined by Eq. (38).

The parity-mixed HF equation (44) defines a complete, orthonormal set of parity-mixed single-particle states, which we now use in a systematic calculation of higher-order correlation corrections. We proceed by constructing the parity-mixed basis states explicitly using the B-spline approach. First, we construct a parity-pure basis set $|i>$ as descibed earlier. Then we generate the opposite-parity admixture $|i_{\rm PNC}>$ for each state by summation over the formal solution to (47):

$$|i_{\rm PNC}>=\sum_j \frac{|j><j|h_{\rm PNC}+V_{\text{PNC-HF}}|i>}{\epsilon_j-\epsilon_i}. \qquad (49)$$

The completeness of the parity-mixed basis set has been checked by various methods as described in our earlier work [25]. We include negative-energy states in the sum over j in (49), which can be important when using the velocity form of the dipole operator (see Sec. IV B). Note that the nonlocal exchange terms in $V_{\rm HF}$ destroy length-velocity equivalence at the PNC-HF stage.

We now consider three classes of correlation corrections to the parity-mixed HF equation, which we have arranged in order of decreasing significance in the following sections. First, we consider the RPA corrections to the dipole operator. The RPA correction contains the entire second-order correction, in a counting scheme in which the parity-mixed HF matrix element is regarded as being of first order, and each subsequent Coulomb correction increases the order by one. Then, we consider the most important third-order corrections, which arise from Brueckner-orbital (BO) modifications to the external valence states. Finally, we add residual third-order corrections including normalization corrections. A summary of the calculation is given in Table VIII.

B. RPA corrections to the dipole operator

The RPA correction to the dipole operator has two parts in parity-mixed MBPT: the usual one Δd, given by (38), and a part $\Delta d_{\rm PNC}$ formed by linearizing (38) in $h_{\rm PNC}$ with the states a and m regarded as being parity mixed. The RPA correction is then

$$E_{\rm PNC}(\text{RPA}) = <7s|\Delta d|6s_{\rm PNC}> + <7s_{\rm PNC}|\Delta d|6s> + <7s|\Delta d_{\rm PNC}|6s>. \qquad (50)$$

Diagrammatically, $\Delta d_{\rm PNC}$ arises from opposite-parity substitutions inside the RPA bubbles. These "internal" substitutions are suppressed because they contain implicitly large energy denominators corresponding to excitation from the tightly bound core. By contrast, the other two terms in (50), which involve substitutions on the external valence lines of the diagrams, contain implicitly small energy denominators corresponding to valence excitations, and dominate the RPA correction.

The well-known length-velocity equivalence for the RPA approximation can be shown to extend to the parity-mixed treatment given here [39, 40], and provides a powerful check on the accuracy of the calculation, in particular the solution of the complicated self-consistent equations defining $\Delta d_{\rm PNC}$. We have obtained length-velocity agreement at the level of one part in 10^5.

C. Brueckner orbital corrections

1. Introduction

The Brueckner orbital (BO) correction to the valence state modifies the valence wave function to take account of the polarization potential set up by the polarization of the core by the valence electron. Formally, the polarization potential is represented by the nonlocal self-energy operator Σ [42], and the modified valence state follows from adding Σ to the HF Hamiltonian and solving for normalized *quasiparticle* valence orbitals ϕ_v and corresponding eigenvalues ϵ'_v [41]:

$$[h_D + V_{\rm nuc} + V_{\rm HF} + \Sigma(\epsilon'_v)]\phi_v = \epsilon'_v\phi_v. \qquad (51)$$

By "self-energy" we refer not to the radiative self-energy, but to a many-body counterpart given by the sum of

all one-particle-irreducible many-body diagrams having one ingoing and one outgoing line [42]. The solution of (51) is then equivalent to summing chains of self-energy diagrams. If Σ were the exact self-energy, ϵ'_v would be the exact ionization energy. The treatment of the self-energy in this way was first advocated in PNC calculations by the Novosibirsk group [37].

In order to make contact with previous work on the BO correction, we consider the solution of (51) in three stages. First, we approximate Σ by the leading term in a perturbative treatment, $\Sigma^{(2)}$, and retain terms linear in $\Sigma^{(2)}$. This stage permits a useful check on numerical methods. Second, we consider the chaining of $\Sigma^{(2)}$ by iterative solution of the quasiparticle equation (51). We find a significant contribution to $E_{\rm PNC}$. Finally, we consider phenomenologically third- and higher-order corrections to Σ, finding them to be quite small.

2. Linear treatment of self-energy

Because $\Sigma^{(1)}$ is part of the HF potential, the leading contribution to Σ in a perturbative treatment is $\Sigma^{(2)}$:

$$< i|\Sigma^{(2)}(\epsilon)|j >= \sum_{amn} \frac{g_{aimn}\tilde{g}_{mnaj}}{\epsilon_a + \epsilon - \epsilon_m - \epsilon_n} - \sum_{abm} \frac{g_{abjm}\tilde{g}_{imab}}{\epsilon_a + \epsilon_b - \epsilon_m - \epsilon}. \quad (52)$$

We first put $\Sigma = \Sigma^{(2)}$ and solve (51) perturbatively to first order in $\Sigma^{(2)}$. The result can be expressed in terms of the lowest-order Brueckner modification $|\delta v >$ to the HF state, $|\phi_v\rangle = |v\rangle + |\delta v\rangle$:

$$|\delta v >= \sum_{j\neq v} \frac{|j >< j|\Sigma^{(2)}(\epsilon_v)|v >}{\epsilon_v - \epsilon_j}. \quad (53)$$

The corresponding third-order matrix element correction is

$$Z^{(3)}_{wv}({\rm BO}) =< \delta w|z|v > + < w|z|\delta v >, \quad (54)$$

for an arbitrary one-body operator z. Calculations of this correction using relativistic basis sets have now been performed by a number of groups for hyperfine constants and dipole matrix elements, and numerical agreement is very good [43, 32, 44].

In the parity-mixed treatment of interest here, Σ separates into a normal and a PNC part, $\Sigma \rightarrow \Sigma + \Sigma_{\rm PNC}$, the latter being given by linearizing (52) in $h_{\rm PNC}$ with the intermediate states regarded as parity mixed. This extra PNC term $\Sigma_{\rm PNC}$ corresponds to opposite-parity substitutions *inside* the self-energy diagram. The valence Brueckner modifications also become parity mixed, $|\delta v >\rightarrow |\delta v > + |\delta v_{\rm PNC} >$. It is useful to distinguish between "internal" and "external" contributions to $|\delta v_{\rm PNC}\rangle$, according to where the opposite-parity substitution is made. Linearizing (53) we obtain

$$|\delta v_{\rm PNC} >= |\delta v_{\rm PNC} >_{\rm ext} + |\delta v_{\rm PNC} >_{\rm int}, \quad (55)$$

$$|\delta v_{\rm PNC} >_{\rm ext} = \sum_{j\neq v} \frac{(|j >< j_{\rm PNC}| + |j_{\rm PNC} >< j|)\,\Sigma^{(2)}(\epsilon_v)|v >}{\epsilon_v - \epsilon_j} + \sum_{j\neq v} \frac{|j >< j|\Sigma^{(2)}(\epsilon_v)|v_{\rm PNC} >}{\epsilon_v - \epsilon_j}, \quad (56)$$

$$|\delta v_{\rm PNC} >_{\rm int} = \sum_{j\neq v} \frac{|j >< j|\Sigma^{(2)}_{\rm PNC}(\epsilon_v)|v >}{\epsilon_v - \epsilon_j}. \quad (57)$$

For each type of correction, internal or external, we define a third-order BO term by

$$E_{\rm PNC}({\rm BO\text{-}3}) =< \delta w_{\rm PNC}|d|v > + < w_{\rm PNC}|d|\delta v > + < \delta w|d|v_{\rm PNC} > + < w|d|\delta v_{\rm PNC} > . \quad (58)$$

After some initial discrepancies, there is now agreement on the values of these terms [25, 32, 45],

$$E_{\rm PNC}({\rm BO\text{-}3,ext}) = -0.058 \times 10^{-11}\, i|e|a_0(-Q_W/N), \quad (59)$$

$$E_{\rm PNC}({\rm BO\text{-}3,int}) = -0.003 \times 10^{-11}\, i|e|a_0(-Q_W/N). \quad (60)$$

This agreement shows that the numerical issues surrounding parity-mixed basis sets are well understood. Once more, the contribution from internal substitutions is small, suppressed by energy-denominator considerations.

3. Nonlinear treatment of self-energy

After linearization in $h_{\rm PNC}$, the parity-mixed quasiparticle equation becomes

$$[\epsilon'_v - h_{\rm D} - V_{\rm nuc} - V_{\rm HF} - \Sigma(\epsilon'_v)]\phi_{v\,\rm PNC} = [h_{\rm PNC} + V_{\rm PNC\text{-}HF} + \Sigma_{\rm PNC}(\epsilon'_v)]\phi_v. \quad (61)$$

Equations (51) and (61) then form a pair analogous to the parity-mixed HF equations (46) and (47). Since $\Sigma_{\rm PNC}$ is so small, we exclude it from (61) and evaluate it in lowest order, as in Eq. (60).

We have developed a procedure for solving the quasiparticle equation (51) and its PNC counterpart (61), with $\Sigma = \Sigma^{(2)}$, by means of a sequence of iterative corrections to the corresponding HF solutions. The scheme is written out in detail for Eq. (51) in Ref. [24], where we considered the chaining contributions to the ionization energy. Typically only four or five iterations in this scheme are necessary to produce adequate convergence.

Having thus obtained ϕ_v and $\phi_{v\,\rm PNC}$ appropriate to $\Sigma = \Sigma^{(2)}$, we take the expectation value of the RPA form of the dipole operator, thereby building in additionally cross terms between the RPA and BO effects. The full BO correction is then taken to be

$$E_{\rm PNC}({\rm BO}) = <\phi_{{\rm PNC}7s}|d+\Delta d|\phi_{6s}> + <\phi_{7s}|d+\Delta d|\phi_{{\rm PNC}6s}> + <\phi_{7s}|\Delta d_{\rm PNC}|\phi_{6s}> - E_{\rm PNC}({\rm PNC\text{-}HF}) - E_{\rm PNC}({\rm RPA}), \quad (62)$$

where we have subtracted the two terms implicit in the first line that we have already discussed. We find $E_{\rm PNC}({\rm BO}) = -0.015$, which is somewhat different from the third-order BO term (59)—a −4.5% reduction when expressed as a percentage of the total $E_{\rm PNC}$. Part of this reduction (−1.5%) is due to the RPA-BO crossterms, but most is due to the chaining (−3%).

4. *Higher-order self-energy*

The effect of the third- and higher-order self-energy may be estimated phenomenologically by rescaling the second-order energy so as to fit experimental ionization energies [37, 32]. This rescaled self-energy retains the correct physical $1/r^4$ behavior at large r. We put $\Sigma = \lambda_{\rm ex}\Sigma^{(2)}$, where the values $\lambda_{\rm ex} = 0.80$ for the s-wave self-energy, and $\lambda_{\rm ex} = 0.84$ for the $p_{1/2}$-wave self-energy, were chosen to reproduce the $6s$, $7s$, $6p_{1/2}$, and $7p_{1/2}$ ionization energies. The smallness of $\lambda_{\rm ex}$ shows that $\Sigma^{(2)}$ considerably overestimates the exact self-energy. However, we find that the final result for $E_{\rm PNC}({\rm BO})$ changes by only a few tenths of a percent after making this rescaling. This result suggests that, while it is essential to chain the self-energy, higher-order treatment of the self-energy itself is less important. This is certainly a significant simplification for future more precise work.

To investigate the effect of the rescaling more systematically, we show in Fig. 4 hyperfine constants, allowed dipole matrix elements, and $E_{\rm PNC}$ as a function of a continuous rescaling, $\Sigma = [(1-\lambda_{\rm ex})\rho + \lambda_{\rm ex}]\Sigma^{(2)}$, described by a parameter ρ which varies from −1 to +1. Use of the energy-fitted rescaling $\lambda_{\rm ex}$ then corresponds to $\rho = 0$, and use of the unscaled self-energy to $\rho = 1$. To compute a standard property for a particular ρ in this figure, we first solve the quasiparticle equation (51) to obtain ϕ_v^ρ, and then evaluate

$$Z_{wv}(\rho) = <\phi_v^\rho|z+\Delta z|\phi_v^\rho> + Z_{wv}({\rm SR}) + Z_{wv}({\rm norm}), \quad (63)$$

where z is the appropriate one-body operator, and Δz is the RPA correction given by (38). The two ρ-independent terms are small structural radiation and normalization terms taken from the all-order procedure of Ref. [27], included to make the comparison with experiment more meaningful. We take the 'experimental' value for $E_{\rm PNC}$ to be the energy-fitted value. The plot shows that for all standard properties, the theoretical value improves significantly when the second-order self-energy is rescaled to fit energies. However, while the rescaling affects hyperfine constants rather dramatically, by nearly 10%, $E1_{\rm PNC}$ changes by only a few tenths of a percent over the whole range of rescalings.

It is rather easy to see why the chaining of the self-energy is so important. If one considers the sum over states (35) implicit in the parity-mixed MBPT procedure, one sees that chaining effectively corrects the energy denominator from its HF value to the physical value—roughly a 10% change. Less obvious is the reason for the insensitivity of $E_{\rm PNC}$ to Σ (or equivalently to ρ), which appears to be due to an accidental, though fortunate, cancellation of numerator corrections with corresponding denominator corrections. We observe that the behavior of weak matrix elements as a function of ρ is similar to that of hyperfine constants; however, the

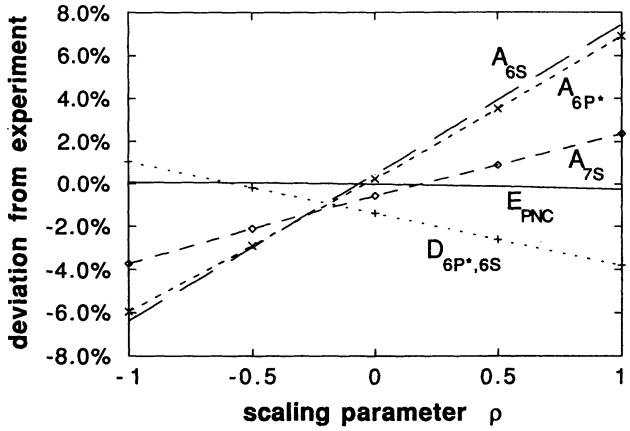

FIG. 4. Effect of a continuous rescaling of the second-order self-energy on the hyperfine constants of the $6S$, $7S$, and $6P_{1/2}$ states, the $6S$-$6P_{1/2}$ allowed dipole matrix element, and the PNC dipole matrix element. The rescaling is described by the parameter ρ (see text for details). The value $\rho = 0$ corresponds to a rescaling of the self-energy to fit ionization energies; when $\rho = 1$, the unscaled second-order self-energy is used.

energy denominator changes in a similar ratio. An analogous cancellation is apparent from the scatter analysis in Table VI, rows 1 and 5.

We give a conservative error estimate on $E_{\rm PNC}({\rm BO}) = -0.015(9)$ because we have found that other ways of modifying $\Sigma^{(2)}$, such as omitting deep core states from the sum in (52), can produce larger changes in $E_{\rm PNC}({\rm BO})$ while giving little change in ionization energies. We also note that from Fig. 4 the agreement with experiment is better for hyperfine constants than for dipole matrix elements, after the rescaling. It is then possible to imagine that, upon rescaling a more exact initial approximation to the self-energy, the whole $E_{\rm PNC}$ curve could be translated.

We note that the Novosibirsk group [32], who originally chained the self-energy in this way, have added an explicit set of higher-order terms to $\Sigma^{(2)}$ using a Green's-function approach, and also find only a small change in the final result. Their final value agrees quite well with ours, as do the individual terms in Table VIII. The effect of the self-energy has also been treated in a semiempirical manner [46], with a result again in agreement with the present calculation.

D. Residual third-order terms

By including the RPA and BO corrections above, we have already evaluated the most important set of third-order terms. We now consider the smaller remaining third-order terms, beginning with those shown in Fig. 2, which we call *structural radiation* (SR) terms following the terminology of Dzuba *et al.* [37]. Only the dipole operator is drawn explicitly; $h_{\rm PNC}$ enters implicitly through the use of parity-mixed single-particle states. We calculate only opposite-parity substitutions on the external valence lines, and neglect substitutions inside each diagram, which are suppressed once again by energy-denominator considerations. The terms produce a small 0.4% correction. We can investigate certain higher-order corrections to these terms by making use of all-order SR dipole matrix elements from Ref. [27], and we use these terms to place an error estimate on this contribution.

Also entering in third order is a term which adjusts the normalization of the wave function as many-body corrections are added. For the matrix element of an arbitrary one-body operator z, this normalization term takes the form, in third order, [37, 16]

$$Z^{(3)}_{wv}({\rm norm}) = -\frac{1}{2} z_{wv} \left(\sum_{amn} \frac{g_{avmn}\tilde{g}_{mnav}}{(\epsilon_a+\epsilon_v-\epsilon_m-\epsilon_n)^2} + \sum_{abm} \frac{g_{abvm}\tilde{g}_{vmab}}{(\epsilon_a+\epsilon_b-\epsilon_m-\epsilon_v)^2} + (v \rightarrow w) \right). \tag{64}$$

We generalize this expression to higher order by using "valence normalization" terms taken from the all-order procedure [27],

$$E_{\rm PNC}({\rm norm}) = -\frac{1}{2} E1_{\rm PNC}({\rm tot})(N^{(a)}_{6S} - N^{(b)}_{6S} + N^{(a)}_{7S} - N^{(b)}_{7S}), \tag{65}$$

where

$$E_{\rm PNC}({\rm tot}) = E_{\rm PNC}({\rm PNC\text{-}HF}) + E_{\rm PNC}({\rm RPA}) + E_{\rm PNC}({\rm BO}), \tag{66}$$

and $N^{(a)}_v$ and $N^{(b)}_v$ are given by the Goldstone diagrams in Fig. 5. Note the minus signs in front of $N^{(b)}_{6S}$ and $N^{(b)}_{7S}$, which cause (65) to reduce to the third-order form (64) [47]. We find $N^{(a)}_{6S} - N^{(b)}_{6S} = 0.0144 - (-0.0004) = 0.015$ and $N^{(a)}_{7S} - N^{(b)}_{7S} = 0.0029 - (-0.0001) = 0.003$, making $E_{\rm PNC}({\rm norm})$ a -0.9% effect. We note that another type of normalization term, which enters in fourth order, has already been included by virtue of using quasiparticle states ϕ_v normalized to unity.

E. Summary

Our result from the parity-mixed MBPT approach, after combining errors in quadrature, is $E_{\rm PNC}(p\ {\rm mix}) = -0.902(9) \times 10^{-11}\, i|e|a_0(-Q_W/N)$, in agreement with the result (39) from the sum-over-states approach. As our final value, we average the results of the two approaches, leaving the theory error unmodified,

$$E_{\rm PNC}({\rm theory}) = -0.905(9) \times 10^{-11}\, i|e|a_0(-Q_W/N). \tag{67}$$

VI. NONLEADING PNC EFFECTS

In this section we address a number of effects that affect the PNC amplitude at the few percent or smaller level. Because these effects are relatively small, all of the calculations use HF level wave functions. We discuss in turn the question of the Breit interaction, the distribution of matter in the nucleus, nuclear spin-dependent contributions, and PNC induced by Z exchange between electrons.

A. Breit correction

Because of the short-distance nature of the weak interaction, relativistic effects are important and the Breit interaction may be enhanced. We find, however, that the Breit correction is small. We include the Breit interaction self-consistently in the HF scheme by generalizing

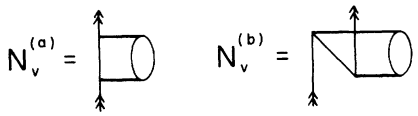

FIG. 5. Diagrams giving the valence normalization. The solid lines represent all-order pair excitation coefficients, as in Ref. [27].

the Coulomb interaction to include the Breit interaction, $g_{ijkl} \rightarrow g_{ijkl} + b_{ijkl}$. The HF potential then acquires an extra term, the "Hartree-Fock-Breit" potential:

$$(h_D + V_{\rm nuc} + V_{\rm HF} + V_{\rm HFB})\psi = \epsilon\psi. \quad (68)$$

The PNC counterpart of this equation is

$$(\epsilon - h_D - V_{\rm nuc} - V_{\rm HF} - V_{\rm HFB})\psi_{\rm PNC}$$

$$= (h_{\rm PNC} + V_{\rm PNC\text{-}HF} + V_{\rm PNC\text{-}HFB})\psi, \quad (69)$$

using a generalization of the notation in Eq. (47). Since the Breit correction is so small, we simplify the calculation by neglecting the term $V_{\rm PNC\text{-}HFB}$ on the RHS of the above. We solve Eq. (69) and use the solution to evaluate the weak-interaction matrix element including the Breit interaction. By comparing with the conventional PNC-HF result, we find a small Breit correction of 0.2%, which is included in Tables VII and VIII.

B. Nuclear density distribution

The weak charge depends on a weighted average of the neutron and proton distributions in the nucleus. The latter distribution can be directly determined from a muonic x-ray experiment [48]. Fitting to an assumed spherical Fermi distribution of

$$\rho_{\rm proton}(r) = \rho_0(1 + e^{-(r-c)/a})^{-1} \quad (70)$$

with $a = 2.3/4\ln 3$, one finds $c = 5.6743(10)$ fm. While the cesium nucleus is not precisely spherical, deviations from sphericity can be shown to be associated with PNC Hamiltonians that admix opposite-parity states with $j \geq 3/2$, which have essentially no overlap with the nucleus and thus produce a negligible effect on $E_{\rm PNC}$. If one assumes that the neutron distribution has exactly the same form as the proton distribution, the lowest-order Hartree-Fock prediction for PNC is

$$E_{\rm PNC} = -0.7396 \times 10^{-11}\, i|e|a_0(-Q_W/N). \quad (71)$$

However, the neutron distribution must at some level differ from the proton distribution, and it is important to include this effect. Because no direct experimental measurement of the neutron distribution is available, we have used a theoretical calculation [49] that reproduces the charge radius of the nucleus and predicts a neutron distribution

$$\rho_{\rm neutron}(r) = \rho_0'(1 + e^{-(r-c')/a'})^{-b}, \quad (72)$$

where $a' = 0.648\,23$ fm, $b = 1.589$, and $c' = 6.153$ fm. Using this distribution in place of Eq. (70) changes -0.7396 in Eq. (71) to -0.7390, a change of -0.08% in magnitude. While it is difficult to assign a theoretical error to nuclear shell model calculations, the small overall size of the effect of using the neutron distribution of Eq. (72) makes the associated theoretical uncertainty unimportant.

Note that the insensitivity to the neutron density discussed above refers to the effect on $E_{\rm PNC}$ for the single isotope ^{133}Cs. Recently, Fortson, Pang, and Wilets [50] have discussed the change in $E_{\rm PNC}$ between a pair of isotopes, and have found an enhanced uncertainty due to the neutron density.

C. Nuclear spin-dependent effects

We have concentrated so far in this paper on one particular part of the exchange of a Z between the nucleus and electrons, but there are three other parts that must be considered. As discussed in Sec. II, atomic PNC is associated with both (A_e, V_N) and (V_e, A_N) interactions, and each of these interactions has a timelike and spacelike component. The Hamiltonian in Eq. (3) is associated with the timelike component of the former interaction after making the usual identification of a potential with the Fourier transform of the matrix element for Z exchange. We estimate that the spacelike component of (A_e, V_N), which gives a nuclear-spin-dependent term, enters at under the 0.1% level. This is because two small factors suppress the nuclear matrix element. The first is the fact that coherence in the sum over nucleons is lost for a vector quantity such as $\boldsymbol{\alpha}_N$, which must be proportional to nuclear spin. All but one nucleon in the cesium nucleus couple to angular momentum zero, so this effect alone would lead to a few percent contribution. However, the nuclear velocity also enters, and because nuclei are fairly well described by nonrelativistic shell models, a further suppression of $v_{\rm nuc}/c$ should make the spacelike component negligible. There is a possible enhancement factor on the electron side because $\boldsymbol{\alpha}\gamma_5$ is diagonal. However, because the electron is quite relativistic inside the nucleus, this enhancement should not be numerically significant.

Turning to the (V_e, A_N) interaction, we note first that this is proportional to $C_{1e} = -\frac{1}{2}(1 - 4\sin^2\theta_W)$, which is quite small at the present value of θ_W. The timelike component of this interaction is further suppressed by the same factors discussed in the previous paragraphs, and is thus completely negligible. The spacelike component, however, is no longer suppressed by a factor of $v_{\rm nuc}/c$, and we treat it here using the Hamiltonian

$$H_W^{(2)} = -\frac{G_F}{\sqrt{2}}\frac{\kappa - \frac{1}{2}}{I(I+1)}\boldsymbol{\alpha}\cdot\mathbf{I}\,\rho(r), \quad (73)$$

where $\kappa = 4$ for the valence proton of ^{133}Cs, and $K_2 \approx -0.05$. However, a numerically more important nuclear spin-dependent effect arises from the *anapole moment* K_a [51], which gives rise to a similar Hamiltonian:

$$H_W^a = \frac{G_F}{\sqrt{2}}K_a\frac{\kappa}{I(I+1)}\boldsymbol{\alpha}\cdot\mathbf{I}\,\rho(r). \quad (74)$$

The anapole moment arises from weak interactions inside the nucleus that allow it to have a parity-violating magnetic moment. We can treat these Hamiltonians together by replacing K_a in Eq. (74) with $K \equiv K_a - (\kappa - \frac{1}{2})/\kappa\, K_2$. We can do this because we have found little sensitivity to the distribution assumed for the distributions $\rho(r)$, which are in principal different.

While the anapole moment is an interesting manifestation of PNC in nuclei, if one is interested in testing radiative corrections to Q_W it is desirable to eliminate

the effect of this moment, the calculation of which involves strong-interaction uncertainties. This can be done because the experiment [5] measures two different transitions: $6S(F=3) \rightarrow 7S(F=4)$ and $6S(F=4) \rightarrow 7S(F=3)$. Linear combinations of these transitions can be taken that either eliminate or isolate nuclear spin-dependent effects. The results quoted for PNC in this paper have followed the convention of assuming a zero spin nucleus, and further assuming the magnetic quantum numbers of the $6S$ and $7S$ states are both $+\frac{1}{2}$. The actual situation, however, has an initial state FM and a final state $F'M'$, and is associated with an angular factor depending on these values: this factor, which is the same for the two transitions, has been taken into account in presenting the experimental data. However, when the spin-dependent Hamiltonians are taken into account, the $F=3 \rightarrow F=4$ and $F=4 \rightarrow F=3$ transitions will be different, partly because the angular factors are now no longer the same, and partly because the atomic structure calculation differs, depending on matrix elements of $\boldsymbol{\alpha}$ rather than γ_5. We have carried out a PNC-HF level calculation incorporating the nuclear spin-dependent Hamiltonians and have found the result

$$E_{\rm PNC} = -0.905(9) i|e|a_0 \times 10^{-11} \left[\left(\frac{Q_W}{-N} \right) + A(F',F)K \right], \tag{75}$$

where A(3,3)=0.029, A(4,3) = −0.041, A(3,4)= 0.048, and A(4,4) = −0.022. These coefficients agree to within 10% with results from other groups [52, 53]. It is then trivial to take linear combinations of the experimental result given in Eq. (6) so as either to cancel the effect of K or to determine it. We will carry out the former operation in Sec. VII, and observe here that the latter operation leads to $K = 0.83(46)$, which is consistent with the result $K = 0.29$–0.37 calculated in Ref. [54]. Further work on the anapole moment has been reported in Refs. [55] and [56]. We also note that the hyperfine interaction taken together with the weak Hamiltonian in Eq. (3) has been shown [57, 58] to act as a third kind of nuclear spin-dependent Hamiltonian, which modifies the effective anapole moment by about 10%.

D. Z exchange between electrons

As the final small effect that could possibly enter at the few tenths of a percent level we turn to parity nonconservation induced by Z exchange between electrons. While expected to be small compared to the basic PNC effect of exchange of a Z between the nucleus and an electron, Z exchange between electrons has the potential of contributing to the experimental result at a significant level. To calculate it we replace the interaction induced by the exchange of a Coulomb photon with that induced by exchange of a Z. Coulomb photon exchange gives rise to the matrix element in Eq. (14): replacing the photon with a Z then gives an analogous weak-interaction matrix element

$$g^w_{ijkl} = \sqrt{2} G_F \int d^3r \bar{\psi}_i(\mathbf{r})(\gamma_\mu C_{1e} + \gamma_\mu\gamma_5 C_{2e})\psi_k(\mathbf{r}) \times \bar{\psi}_j(\mathbf{r})(\gamma^\mu C_{1e} + \gamma^\mu\gamma_5 C_{2e})\psi_l(\mathbf{r}), \tag{76}$$

where $C_{1e} = -\frac{1}{2}(1 - 4\sin^2\theta_W)$ and $C_{2e} = \frac{1}{2}$. If we make the replacement $g_{ijkl} \rightarrow g_{ijlk} + g^w_{ijkl}$ in the formula for the first-order correction to a dipole matrix element given in Eq. (29), and work to first order in g^w, we find a PNC matrix element

$$E_{\rm PNC}({\rm EE}) = \sum_{a,i\neq v} \frac{d_{wi}\tilde{g}^w_{iava}}{\epsilon_v - \epsilon_i} + \sum_{a,i\neq w} \frac{d_{iv}\tilde{g}^w_{waia}}{\epsilon_w - \epsilon_i} + \sum_{am} \frac{d_{am}\tilde{g}^w_{wmva}}{\epsilon_{av} - \epsilon_{mw}} + \sum_{am} \frac{d_{ma}\tilde{g}^w_{wavm}}{\epsilon_{aw} - \epsilon_{mv}}, \tag{77}$$

with only the cross terms proportional to $C_{1e}C_{2e}$ in Eq. (76) contributing. The evaluation of this expression is straightforward but lengthy, the main difficulty being the three-vector part of Eq. (76), which can be evaluated using methods developed for calculating the Breit interaction described in the appendices of Ref. [59]. However, the exchange and direct contributions are related by a Fierz identity, $\tilde{g}^w_{ijkl} = 2g^w_{ijkl}$, which can be used to reduce the calculation to the relatively easy-to-evaluate direct terms [the three-vector part of Eq. (76) vanishes for the first two terms of Eq. (77)]. It is then found that the last two terms of Eq. (77) are completely negligible, but that the first two contribute

$$E_{\rm PNC}({\rm EE}) = 0.0086 C_{1e} \times 10^{-11}\, i|e|a_0(-Q_W/N), \tag{78}$$

where in the sum over core states a, the $1s$ state contributes more than 80% of the result. Using $\sin^2\theta_W = 0.2323$ in the above gives the small correction

$$E_{\rm PNC}({\rm EE}) = -0.000\,30 \times 10^{-11}\, i|e|a_0(-Q_W/N), \tag{79}$$

an additive 0.03% contribution to the theoretical prediction that should in principle be removed before extracting Q_W. Given the relatively much larger theoretical uncertainties from other sources discussed above, however, we see that Z exchange between electrons can be safely neglected.

VII. DETERMINATION OF THE WEAK CHARGE

We now extract the experimental value of the weak charge Q_W from our theoretical prediction (67), $E_{\rm PNC} = -0.905(9) \times 10^{-11}\, i|e|a_0(-Q_W/N)$, and the experimental measurement [5] of Eq. (6). In order to minimize nuclear uncertainties we take a linear combination of the two transitions as described in Sec. VI C. Using $\beta = 27.00[20]a_0^3$ and the conversion factor

$$\frac{|e|}{a_0^2} = 5.1422 \times 10^{12}\ \frac{\rm mV}{\rm cm} \tag{80}$$

in Eq. (6) then gives

$$E_{\rm PNC}^{\rm expt} = -0.8252(184)[61] \times 10^{-11}\, i|e|a_0(-Q_W/N). \tag{81}$$

Combining Eqs. (81) and (5) then gives our principal result

$$Q_W = -71.04(1.58)[0.88], \tag{82}$$

where the first error is experimental, and the second theoretical. Before discussing the particle-physics implications of this determination, we present an analysis of the reliability of the quoted theoretical error [0.88] and the prospects of reducing it further.

A. Reliability of atomic theory

Given the important consequences for particle theory of PNC in cesium, it is necessary to provide a critical analysis of our claimed theory error of 1%. What we have presented in this paper is a calculation that definitely misses diagrams contributing at the several tenths of a percent level. In the sum-over-states approach, we have used these discrepancies to test the stability of the PNC prediction by performing the set of rescalings described in Sec. IV B. The rescalings are essentially an approximate way of putting in higher-order diagrams not yet included rigorously. By examining the effect of the rescalings on $E_{\rm PNC}$, we can then infer the likely size of omitted correlation effects. We do this by carrying out the rescalings in several different ways and observing the scatter of results. As can be seen from Fig. 3, the various results clustered within 1% of one another. Note that we do not attempt to use these modifications to improve our calculation, merely to estimate the theory error, which thus represents an estimate of the extent to which we cannot calculate $E_{\rm PNC}$ entirely from first principles. We have also carried out the PNC calculation a different way, by using parity-mixed MBPT. The errors assigned to the various terms in this alternative approach are given by the detailed arguments in Sec. V. Because the two approaches are so different, and group the various contributions in different ways, the agreement between them forms an important additional check on the accuracy of the calculation.

With the accuracy of the atomic theory now at the 1% level, it is important to ask what the prospects are for another order of magnitude of improvement. We have indicated several extensions to our techniques which we feel are feasible and which we expect to improve upon our present accuracy by up to an order of magnitude. These techniques essentially involve accounting for triple excitations completely in our all-order procedure. Perhaps the hardest task, however, is to give a convincing demonstration that a particular level of error in $E_{\rm PNC}$ has indeed been achieved. The most reliable gauge of theory error remains the prediction of the standard properties, which in the case of ionization energies and hyperfine constants are still known experimentally with greater precision than our present theory. If all known properties of cesium could be reproduced by some *ab initio* calculational scheme to within about 0.1%, we feel it would be reasonable to trust a PNC calculation carried out in the same fashion to this same level, subject to a scatter analysis along the lines presented above. Note that hyperfine splittings must be included in this argument because of their similarity to PNC. It is quite possible that a calculation that gives good energies, which depend on wave functions at typical atomic distances, could give poor results for quantities sensitive to nuclear distance scales. The main danger in this scheme is a high-order diagram that somehow does not contribute either to energies or to hyperfine splitting that does give a large contribution to PNC. This possibility cannot be dismissed, but we note that, for the calculations carried out so far, PNC is actually less sensitive to missed diagrams than the hyperfine splitting.

It must not be forgotten that the vector transition polarizability β is also crucial in interpreting PNC in cesium. The *ab initio* calculation of β is not straightforward, the accuracy of our present calculation being comparable to that of $E_{\rm PNC}$. Here, however, one can make good use of empirical information, because β depends only on allowed dipole matrix elements and energies. Moreover, β itself can in principle be measured directly, or else inferred from experiment with minimal theoretical input using the method of Bouchiat and Guena [35]. We encourage further experimental work in this direction.

VIII. COMPARISON WITH EXPERIMENT AND CONSEQUENCES FOR PARTICLE PHYSICS

When a single weak-interaction result is known, its interpretation is generally made ambiguous because of the unknown values of the weak angle θ_W, the top-quark mass m_t, and the Higgs-boson mass M_H. For example, the radiatively corrected weak charge is approximately given by the formula

$$Q_W \approx \left(0.9796 + 0.0020\frac{m_t^2}{m_W^2}\right) \times\{-N + Z[1 - 4.012\sin^2\hat{\theta}_W(m_W)]\}. \tag{83}$$

This assumes a Higgs-boson mass of 100 GeV, but deviations of the Higgs-boson mass from this value affect the formula only weakly. The exact expression this equation approximates is given in Ref. [60]. It is possible to extract the weak angle from Q_W for a given top-quark mass, finding, for example,

$$\sin^2\hat{\theta}_W(m_W) = \begin{cases} 0.2242\,(65), & m_t = 100\ \text{GeV}, \\ 0.2215\,(65), & m_t = 200\ \text{GeV}. \end{cases} \tag{84}$$

It is notable that the same variation in $\sin^2\theta_W$ is found when the top-quark mass is varied from 100 to 200 GeV as was found in Eq. (1). In fact, if the value of $\sin^2\theta_W$ from that equation is used in Eq. (83), it can be seen that the resultant value of Q_W is essentially unchanged. A convenient way of seeing this in more generality is to use the formula [7]

$$Q_W = -73.20(13) - 0.8S - 0.005T. \tag{85}$$

The quantities S and T can be associated with new

physics, with S referring to physics that conserves weak isospin, and T to physics that breaks weak isospin. Even in the absence of new particles these quantities vanish only for $m_t = 140$ GeV and $m_H = 100$ GeV, and

$$T \approx 0.257 \frac{m_t^2 - (140\ \text{GeV})^2}{m_W^2} - 0.155 \ln\left(\frac{m_\text{H}}{100\ \text{GeV}}\right) \tag{86}$$

and

$$S = 0.053 \ln\left(\frac{m_\text{H}}{100\ \text{GeV}}\right). \tag{87}$$

The smallness of the coefficient of T in Eq. (85) is accidental, depending on the particular numbers of neutrons and protons in the cesium nucleus. We note that the insensitivity of Q_W to the top-quark mass has also been shown by Sandars [61]. Therefore, now that the Z mass has been accurately measured, if one makes the assumption that there is no new physics beyond the standard model, a completely unambiguous prediction for Q_W can be made for cesium:

$$Q_W = -73.20(13). \tag{88}$$

This is consistent with the present value in Eq. (82), but the relatively large experimental and theoretical errors in cesium PNC clearly both need to be reduced.

While the theoretical and experimental errors associated with atomic PNC are still fairly large, the fact that the magnitude measured for Q_W is less than the theoretical prediction in the absence of new physics already has consequences for technicolorlike theories. This is because the new doublets predicted in these theories lead to a positive S, with $S \approx 2$. This would predict $Q_W \approx -74.8$, which is almost three experimental standard deviations away from the present determination. If the central value does not change, a reduction of even a factor of 2 in experimental accuracy would basically rule out such theories if one assumes no extra physics. It is however, possible to imagine scenarios in which extra Z bosons are also present. Because these change the tree-level structure of the theory, Q_W is changed in a way that can mimic a negative S. A number of theories that can accommodate $|Q_W| < 72$ have recently been presented by Langacker and Luo [62]. Because the new physics that is being sought in electroweak physics may be complicated, it is important to have as many probes of it as possible. Accurate determination of the W mass, asymmetry measurements, e–C scattering, etc., should all be pursued. We hope to have shown in this paper that, despite the difficulty of the atomic calculations, cesium PNC can be taken as one of this set of high-accuracy tests of electroweak physics, and can play a role in helping to understand the structure of this theory at the TeV mass scale.

ACKNOWLEDGMENTS

We would like to acknowledge helpful conversations with Victor Flambaum, Paul Langacker, Ingvar Lindgren, William Marciano, Ann-Marie Mårtensson-Pendrill, Carol Tanner, and Carl Wieman, and thank Claude Guet for providing neutron distributions for ^{133}Cs. This research was supported in part by NSF Grant No. PHY90-12408, and partly under the auspices of the U.S. Department of Energy by Lawrence Livermore National Laboratory under Contract No. W-7405-Eng-48. J.S. would like to acknowledge the support of LLNL, where some of his work was done. The calculations were carried out on the National Center for Supercomputer Applications Cray-2.

[1] Particle Data Group, J.J. Hernández *et al.*, Phys. Lett. B **239**, 1 (1990).
[2] W.A. Bardeen, A.J. Buras, D.W. Duke, and T. Muta, Phys. Rev. D **18**, 3998 (1978); E.G. Floratos, D.A. Ross, and C.T. Sachrajda, Nucl. Phys. **B129**, 66 (1977); **B139**, 545(E) (1978).
[3] W. Marciano (private communication).
[4] M.A. Bouchiat and C. Bouchiat, J. Phys. (Paris) **35**, 899 (1974).
[5] M.C. Noecker, B.P. Masterson, and C.E. Wieman, Phys. Rev. Lett. **61**, 310 (1988).
[6] Michael E. Peskin and Tatsu Takeuchi, Phys. Rev. Lett. **65**, 964 (1990).
[7] W. Marciano and J. Rosner, Phys. Rev. Lett. **65**, 2963 (1990).
[8] See the review by E.D. Commins, Phys. Scr. **36**, 468 (1987); M.J.D. Macpherson, K.P. Zetie, R.B. Warrington, D.N. Stacey, and J.P. Hoare, Phys. Rev. Lett. **67**, 2784 (1991).
[9] S.A. Blundell, W.R. Johnson, and J. Sapirstein, Phys. Rev. Lett. **65**, 1411 (1990).
[10] M.A. Bouchiat *et al.*, Phys. Lett. **117B**, 358 (1982).
[11] M.A. Bouchiat *et al.*, Phys. Lett. **134B**, 463 (1984).
[12] M.A. Bouchiat *et al.*, J. Phys. (Paris) **47**, 1709 (1986).
[13] S.L. Gilbert and C.E. Wieman, Phys. Rev. A **34**, 792 (1986).
[14] M. A. Bouchiat and C. Bouchiat, Phys. Lett. **48**, 111 (1974); J. Phys. (Paris) **35**, 899 (1974); **36**, 493 (1975).
[15] J. Sucher, Int. J. Quant. Chem. **24**, 3 (1984).
[16] S.A. Blundell, D.S. Guo, W.R. Johnson, and J. Sapirstein, At. Data Nucl. Data Tables **37**, 103 (1987).
[17] M. Gell-Mann and F. Low, Phys. Rev. **84**, 350 (1951).
[18] J. Sucher, Phys. Rev. **107**, 1448 (1957).
[19] J. Sapirstein, Phys. Scr. **36**, 801 (1987).
[20] W.R. Johnson, S.A. Blundell, and J. Sapirstein, Phys. Rev. A **37**, 307 (1988).
[21] A. Chodos, R.L. Jaffe, K. Johnson, C.B. Thorn, and V.F. Weisskopf, Phys. Rev. D **9**, 3471 (1974).
[22] C. DeBoer, *A Practical Guide to Splines* (Springer, New York, 1978).
[23] S.A. Blundell, W.R. Johnson, Z.W. Liu, and J. Sapirstein, Phys. Rev. A **39**, 3768 (1989).
[24] S. A. Blundell, W. R. Johnson, and J. Sapirstein, Phys. Rev. A **38**, 4961 (1988).

[25] W.R. Johnson, S.A. Blundell, Z.W. Liu, and J. Sapirstein, Phys. Rev. A **37**, 1395 (1988).
[26] S.A. Blundell, W.R. Johnson, and J. Sapirstein, Phys. Rev. A **40**, 2233 (1989).
[27] S.A. Blundell, W.R. Johnson, and J. Sapirstein, Phys. Rev. A **43**, 3407 (1991).
[28] F. Coester, Nucl. Phys. **1**, 421 (1958); F. Coester and H. Kümmel, Nucl. Phys. **17**, 477 (1960).
[29] C. Bouchiat and C.-A. Piketty, Europhys. Lett. **2**, 511 (1986).
[30] J. Hoffnagle *et al.*, Phys. Lett. **85A**, 143 (1981); S.L. Gilbert, R.N. Watts, and C.E. Wieman, Phys. Rev. A 27, 581 (1983); M. A. Bouchiat *et al.*, Optics Commun. **45**, 35 (1983); **46**, 185 (1983).
[31] R.N. Watts, S.L. Gilbert, and C.E. Wieman, Phys. Rev. A **27**, 2769 (1983).
[32] V. A. Dzuba, V. V. Flambaum, and O. P. Sushkov, Phys. Lett. A **141**, 147 (1989).
[33] M.A. Bouchiat, J. Guena, and L. Pottier, J. Phys. (Paris) Lett. **45**, L523 (1984).
[34] J. Hoffnagle, V. L. Telegdi, and A. Weis, Phys. Lett. **86A**, 457 (1981).
[35] M. A. Bouchiat and J. Guena, J. Phys. (Paris) **49**, 2037 (1988).
[36] P. G. H. Sandars, J. Phys. B **10**, 2983 (1977).
[37] V. A. Dzuba, V. V. Flambaum, P. G. Silvestrov, and O. P. Sushkov, Physica Scripta **35**, 69 (1987); J. Phys. B **20**, 3297 (1987).
[38] S. A. Blundell, A. C. Hartley, Z. Liu, A.-M. Mårtensson-Pendrill, and J. Sapirstein, Theor. Chim. Acta **80**, 257 (1991).
[39] A.-M. Mårtensson-Pendrill, J. Phys. (Paris) **46**, 1949 (1985).
[40] W. R. Johnson, D. S. Guo, M. Idrees, and J. Sapirstein, Phys. Rev. A **34**, 1043 (1986).
[41] A.B. Migdal, *Theory of Finite Fermi Systems and Applications to Atomic Nuclei* (Interscience, New York, 1967).
[42] A.L. Fetter and J.D. Walecka, *Quantum Theory of Many-Particle Systems* (McGraw-Hill, New York, 1971).
[43] W.R. Johnson, M. Idrees, and J. Sapirstein, Phys. Rev. A **35**, 3218 (1987).
[44] A. C. Hartley and A.-M. Mårtensson-Pendrill, Z. Phys. D **15**, 309 (1990).
[45] A. C. Hartley, E. Lindroth, and A.-M. Mårtensson-Pendrill, J. Phys. B **23**, 3417 (1990).
[46] A.C. Hartley and P.G.H. Sandars, J. Phys. B **23**, 1961 (1990).
[47] The minus sign may appear at first sight to be at variance with a binomial expansion of the denominator of Eq. (23) in Ref. [27]. However, in the present formulation we include as normalization an additional term arising from $M^{(e)}$ in Eq. (30) of Ref. [27], which reverses the sign in (65).
[48] R. Engfer *et. al.*, At. Data Nucl. Data Tables **14**, 479 (1974).
[49] M. Brack, C. Guet, and H.-B. Hakansson, Phys. Rep. **123**, 275 (1985).
[50] E. N. Fortson, Y. Pang, and L. Wilets, Phys. Rev. Lett. **65**, 2857 (1990).
[51] Ya. Zel'dovich, Zh. Eksp. Teor. Fiz. **33**, 1531 (1957) [Sov. Phys. JETP **6**, 1184 (1958)].
[52] P.A. Frantsuzov and I.B. Khriplovich, Z. Phys. D **7**, 297 (1988).
[53] A. Ya. Kraftmakher, Phys. Lett. A **132**, 167 (1988).
[54] V.V. Flambaum, I.B. Kriplovich, and O.P. Sushkov, Phys. Lett. **146B**, 367 (1984).
[55] W.C. Haxton, E.M. Henley, and M.J. Musolf, Phys. Rev. Lett. **63**, 949 (1989).
[56] C. Bouchiat and C.A. Piketty, Z. Phys. C **49**, 91 (1991); Phys. Lett. B **269**, 195 (1991).
[57] M.G. Kozlov, Phys. Lett. A **130**, 426 (1988).
[58] V.V. Flambaum and I.B. Khriplovich, Zh. Eksp. Teor. Fiz. **89**, 1505 (1985) [Sov. Phys. JETP **62**, 872 (1985)].
[59] W.R. Johnson, S.A. Blundell, and J. Sapirstein, Phys. Rev. A **37**, 2764 (1988).
[60] W. Marciano and A. Sirlin, Phys. Rev. D **29**, 75 (1984).
[61] P.G.H. Sandars, J. Phys. B **23**; L655 (1990).
[62] P. Langacker and M. Luo, Phys. Rev. D **45**, 278 (1992).